

BULLETIN N° 205
ACADÉMIE EUROPÉENNE
INTERDISCIPLINAIRE
DES SCIENCES
INTERDISCIPLINARY EUROPEAN ACADEMY OF SCIENCES



Lundi 2 mai 2016 à 17h :

à la Maison de l'AX, 5 rue Descartes 75005 Paris

Préparation du prochain colloque "Les signatures de la conscience":

Conférence de notre collègue le Professeur Didier DESOR

Membre de la section AEIS de Nancy

Professeur Émérite de l'Université de Lorraine

CNRS et INRA/Éthologie, neurosciences du comportement et sciences cognitives

« *Se percevoir, se percevoir dans l'environnement* »

Notre Prochaine séance aura lieu le lundi 6 juin 2016 à 17h

à la Maison de l'AX, 5 rue Descartes 75005 Paris

Elle aura pour thème:

Préparation du prochain colloque "Les signatures de la conscience":

Conférence de la Professeure Barbara DEMENEIX

UMR 7221 CNRS

Directeur du Département Régulations et Développement

Muséum National d'Histoire Naturelle (MNHN)

"Hormone thyroïdienne: de l'évolution du cerveau à la perturbation endocrinienne

ACADÉMIE EUROPÉENNE INTERDISCIPLINAIRE DES SCIENCES INTERDISCIPLINARY EUROPEAN ACADEMY OF SCIENCES

PRÉSIDENT : Pr Victor MASTRANGELO
VICE PRÉSIDENT : Pr Jean-Pierre FRANÇOISE
VICE PRÉSIDENT BELGIQUE(Liège):
 Pr Jean SCHMETS
VICE PRÉSIDENT ITALIE(Rome):
 Pr Ernesto DI MAURO
SECRÉTAIRE GÉNÉRALE : Irène HERPE-LITWIN
TRÉSORIÈRE GÉNÉRALE: Édith PERRIER

MEMBRES CONSULTATIFS DU CA :
 Gilbert BELAUBRE
 François BÉGON
 Bruno BLONDEL
 Michel GONDRAN

COMMISSION FINANCES: Claude ELBAZ
COMMISSION MULTIMÉDIA: Pr. Alain CORDIER
COMMISSION ÉDITION:
 Pr Robert FRANCK et Pr Pierre NABET
COMMISSION SYNTHÈSES SCIENTIFIQUES:
 Jean-Pierre TREUIL
COMMISSION CANDIDATURES:
 Pr. Jean-Pierre FRANÇOISE

PRÉSIDENT FONDATEUR : Dr. Lucien LÉVY (†)
PRÉSIDENT D'HONNEUR : Gilbert BELAUBRE

CONSEILLERS SCIENTIFIQUES :
SCIENCES DE LA MATIÈRE : Pr. Gilles COHEN-TANNOUJJI
SCIENCES DE LA VIE ET BIOTECHNIQUES : Pr Ernesto DI MAURO

CONSEILLERS SPÉCIAUX:
ÉDITION: Pr Robert FRANCK
AFFAIRES EUROPÉENNES :Pr Jean SCHMETS
RELATIONS VILLE DE PARIS et IDF:
 Michel GONDRAN ex-Président
MOYENS MULTIMÉDIA et RELATIONS UNIVERSITÉS:
 Pr Alain CORDIER
RELATIONS AX et MÉCÉNAT : Gilbert BELAUBRE

SECTION DE NANCY :
PRÉSIDENT : Pr Pierre NABET

mai 2016

N°205

TABLE DES MATIÈRES

p. 03 Séance du 2mai 2016
 p. 06 Annonces
 p. 07 Documents

Prochaine séance : lundi 6 juin 2016

Préparation du prochain colloque "Les signatures de la conscience":

Conférence de la Professeure Barbara DEMENEIX

UMR 7221 CNRS

Directeur du Département Régulations et Développement

Muséum National d'Histoire Naturelle (MNHN)

"Hormone thyroïdienne: de l'évolution du cerveau à la perturbation endocrinienne"

Académie Européenne Interdisciplinaire des Sciences
 Siège Social : 5 rue Descartes 75005 Paris
 Nouveau Site Web : <http://www.science-inter.com>

ACADEMIE EUROPEENNE INTERDISCIPLINAIRE DES SCIENCES
5, rue Descartes 75005 Paris

Séance du Lundi 2 mai 2016 5 rue Descartes 75005 Paris à 17h

La séance est ouverte à 17h sous la **Présidence de Victor MASTRANGELO** et en la présence de nos Collègues Gilbert BELAUBRE, Jean-Louis BOBIN, Alain CARDON, Gilles COHEN-TANNOUDJI, Ernesto DI MAURO, Françoise DUTHEIL, Claude ELBAZ, Jean -Pierre FRANCOISE, Michel GONDRAN, Irène HERPE-LITWIN, Antoine LONG, Claude MAURY, Edith PERRIER, Jean SCHMETS Jean-Pierre TREUIL.

Etaient excusés François BEGON, Jean-Pierre BESSIS, Bruno BLONDEL, Michel CABANAC, Alain CORDIER, Juan-Carlos CHACHQUES, Daniel COURGEAU, Vincent FLEURY, Robert FRANCK, Jacques HENRI-ROBERT, Dominique LAMBERT, Gérard LEVY, Jacques LEVY, Valérie LEFEVRE-SEGUIN, Pierre MARCHAIS, Anastassios METAXAS, Jacques NIO, Pierre PESQUIES, Michel SPIRO, Alain STAHL, Jean VERDETTI.

Etait présente en tant que membre correspondant: Marie Françoise PASSINI

I. Présentation de notre collègue conférencier Didier DESORS, membre de la section de l'AEIS NANCY

Notre collègue Didier DESOR est Professeur émérite des universités en *Sciences Cognitives et Comportementales* à l'Université de Lorraine à NANCY, Faculté des Sciences et de Technologies.

Il a exercé des fonctions d'enseignement suivantes pendant toute sa carrière:

- Université de Lorraine
- *Faculté des Sciences de Nancy* : maîtrises, puis masters de biologie et physiologie (sous leurs différentes appellations successives)
- *Faculté des Lettres et Sciences Humaines* : Licence de psychologie (enseignements de biologie générale et d'éthologie)
- *Faculté de médecine* : éthologie dans le cursus d'orthophonie
- **2009-2014** : Interventions (Analyse statistique des données) aux Universités de Rabat, Annaba, Monastir
- Dans le cadre du programme Tempus Euro-maghrébin « **Agro-Ressources Fonctionnelles** » (10 Universités : U. de Lorraine, U. de Montpellier, U. de Pise, U. d'Almeria, U. de Monastir, U. de Jendouba, U. d'Oran, U. d'Annaba, U. de Kenitra, U7. de Rabat).
- **Actuellement : quelques séminaires :**
- *Données actuelles sur l'ontogenèse cérébrale* : Diplôme d'Université « Troubles Spécifiques des Apprentissages », Faculté de médecine, Nancy.
- *Evolutions récentes de la législation et de l'éthique en matière d'expérimentation animale* (Ecole de Chirurgie, Nancy)

Il a également exercé des fonctions de recherche dans des Etablissements publics scientifiques et techniques:

- 1988- 2000 : Centre National de la Recherche Scientifique.(CNRS) : URA 1293 « Aspects fonctionnels et Développement des Comportements »

- 2005 -2012 : Institut National de la Recherche Agronomique (INRA) : URAFPA : Unité de Recherche « Animal, Fonctionnalité des Produits Animaux ».

Ses principaux domaines de compétence sont:

- Analyse du comportement
- Comportement général (apprentissage, mémoire, anxiété, stress, comportement social) du rat
- Plans expérimentaux, analyse statistique des données biologiques
- Etudes pré-cliniques : élaboration, exploitation des données recueillies.

Il travaille actuellement sur:

- *Relations entre les odeurs et les couleurs évoquées (dans le cadre du packaging)*

Il est l'auteur de nombreuses publications récentes internationales à comité de lecture et de 6 ouvrages, il été sollicité pour participer à une dizaine de conférences internationales dans des pays d'Asie, d'Amérique ou d'Europe ou des comités d'expertise pour des grands groupes industriels européens ou nord-américains. Il a également participé à la réalisation de deux films universitaire dont l'un a reçu le Grand Prix du *Festival du Film Universitaire Pédagogique, Lyon, 2012*. Il est également intervenu dans des médias "grand public" ou dans des manifestations comme le Grand Palais..

Très engagé dans la vie associative, il est entre autres :

- **Vice-président** du Comité Meurthe et Moselle de la Ligue contre le Cancer
- **Secrétaire** de « *Espoir 54* » (Accompagnement, réhabilitation et participation à la citoyenneté des personnes en situation de handicap psychique).
- **Membre** de la Commission de suivi des Recherches de la Fondation John Bost (Accueil de polyhandicapés profonds)¹ (La Force, Dordogne)
- **Administrateur** de l'Association des Groupes de Recherche en Stress et Santé
- **Membre de la Commission** des Sites et Paysages Naturels (Préfecture de Région, Metz) (Commission de la Faune Sauvage Captive)
- **Anc^t. Vice-président** du CREA (Centre Régional d'Etudes et d'Actions en faveur des Personnes Inadaptées de Lorraine (Nomination par la Préfecture de région).
- **Anc^t.Président** du Comité d'Ethique et Scientifique du CREA (Centre Régional d'Etudes et d'Actions en faveur des Personnes Inadaptées de Lorraine).

II. Conférence de notre collègue Didier DESOR « *Se percevoir, se percevoir dans l'environnement* »

Nous vous communiquons à nouveau le résumé de son intervention:

Résumé:

Une condition nécessaire de la conscience est la perception de l'état de son propre organisme, ainsi que d'un certain nombre de caractéristiques de l'environnement.

Le système nerveux central ne peut percevoir ces environnements (intérieur et extérieur) que par l'intermédiaire de capteurs et de transducteurs qui détectent, puis convertissent différentes formes d'énergie (mécanique, électromagnétique, chimique...) dans le « langage » propre au système nerveux, c'est-à-dire en variations de potentiels membranaire des neurones. Cet exposé passera en revue les principaux types de récepteurs rencontrés dans le monde

¹ Il s'agit en l'occurrence d'un programme destiné à ouvrir à la communication des personnes porteuses de polyhandicaps sévères, pour lesquelles la motricité est éventuellement réduite à l'extrême (« locked-in syndrome »). Le principe est de leur fournir des tablettes communicantes reliées par un réseau wi-fi dédié, et commandées par les fixations du regard. Les premiers essais sont en cours.

animal, les principes des transductions mises en œuvre, et illustrera quelques-uns des rôles de ces dispositifs dans l'adaptation des organismes à leur environnement.

Pour compléter sa conférence notre collègue Didier DESOR nous conseille la lecture des ouvrages suivants:

Stéphane TANZARELLA (2006) : perception et communication chez les animaux
Ed. De Boeck, Bruxelles, Paris.

Jose Bermudez (2007). The Object Properties Model of Object Perception: Between the Binding Model and the Theoretical Model. Journal of Consciousness Studies 14 (s 9-10):43-65.

Un compte-rendu détaillé sera prochainement disponible sur le site de l'AEIS , <http://www.science-inter.com>.

Notre Président Victor MASTRANGELO procède ensuite à la clôture de cette riche séance.

Irène HERPE-LITWIN

Annonces

- I. L'AEIS a le plaisir de vous annoncer la disponibilité en téléchargement gratuit au format PDF de son ouvrage sur le thème du colloque AEIS-2014 "SYSTEMES STELLAIRES ET PLANÉTAIRES- CONDITIONS D'APPARITION DE LA VIE" sur le site d'EDP-Sciences:**

<http://www.edp-open.org/images/stories/books/fulldl/Formation-des-systemes-stellaires-et-planetaires.pdf>

Documents

Pour préparer la conférence de la Pr Barbara DEMENEIX , nous vous proposons :

- p.08 : un article cosigné par Barbara DEMENEIX paru dans Stem Cell Article / Cell Press intitulé "*Thyroid Hormone Signaling Acts as a Neurogenic Switch by Repressing Sox2 in the Adult Neural Stem Cell Niche*"

Notre collègue Michel GONDRAN qui a présenté lors de notre dernier colloque "Ondes, Matières et Univers" un poster en collaboration avec son fils Alexandre GONDRAN nous a communiqué deux articles:

- p.21 : une présentation au Palais de la Découverte en février 2016 de "Mécanique quantique; deux interprétations " paru dans la revue Découverte N° 402 janvier-février 2016.
- p.31 : un article paru en avril 2016 dans la revue "Foundations of Physics" DOI 10.1007/s10701-016-0011-1 d'avril 2016 (Springer Verlag) cosigné par Alexandre et Michel GONDRAN , intitulé:" *Replacing the Singlet Spinor of the EPR-B Experiment in the Configuration Space with Two Single-Particle Spinors in Physical Space*"

Thyroid Hormone Signaling Acts as a Neurogenic Switch by Repressing Sox2 in the Adult Neural Stem Cell Niche

Alejandra López-Juárez,^{1,4,5} Sylvie Remaud,^{1,5} Zahra Hassani,² Pascale Jolivet,¹ Jacqueline Pierre Simons,¹ Thomas Sontag,¹ Kazuaki Yoshikawa,³ Jack Price,² Ghislaine Morvan-Dubois,^{1,6} and Barbara A. Demeneix^{1,6,*}

¹UMR CNRS 7221, Evolution des Régulations Endocriniennes, Département Régulations, Développement et Diversité Moléculaire, Muséum National d'Histoire Naturelle, 75231 Paris, France

²Centre for the Cellular Basis of Behaviour, The James Black Centre, King's College London, Institute of Psychiatry, 125 Cold Harbour Lane, London SE5 9NU, UK

³Laboratory of Regulation of Neuronal Development, Institute for Protein Research, Osaka University, Osaka 565-0871, Japan

⁴Polyplus Transfection, Boulevard Sébastien Brant, BP 90018 67400 Illkirch, France

⁵These authors contributed equally to this work

⁶These authors contributed equally to this work

*Correspondence: bdem@mnhn.fr

DOI 10.1016/j.stem.2012.04.008

SUMMARY

The subventricular zone (SVZ) neural stem cell niche contains mixed populations of stem cells, transit-amplifying cells, and migrating neuroblasts. Deciphering how endogenous signals, such as hormones, affect the balance between these cell types is essential for understanding the physiology of niche plasticity and homeostasis. We show that Thyroid Hormone (T_3) and its receptor, $TR\alpha 1$, are directly involved in maintaining this balance. $TR\alpha 1$ is expressed in amplifying and migrating cells. *In vivo* gain- and loss-of-function experiments demonstrate first, that $T_3/TR\alpha 1$ directly repress *Sox2* expression, and second, that $TR\alpha 1$ overexpression in the niche favors the appearance of DCX+ migrating neuroblasts. Lack of $TR\alpha$ increases numbers of SOX2+ cells in the SVZ. Hypothyroidism increases proportions of cells in interphase. Thus, in the adult SVZ, $T_3/TR\alpha 1$ together favor neural stem cell commitment and progression toward a migrating neuroblast phenotype; this transition correlates with $T_3/TR\alpha 1$ -dependent transcriptional repression of *Sox2*.

INTRODUCTION

Neural stem cells (NSCs) are defined by their ability to self-renew and differentiate, giving rise to progenitor cells, then neurons, oligodendrocytes, and astrocytes (Doetsch et al., 2002). A controlled balance of proliferation and differentiation is required to maintain homeostasis of the neural stem niche and the proportions of stem cells (type B cells), transit-amplifying progenitors (TAPs or type C cells), and migrating neuroblasts (type A cells) (Doetsch et al., 1999). An important question is how hormone signaling modulates adult stem/progenitor cell

function, thereby affecting the physiological plasticity of adult neurogenesis. The biologically active form of thyroid hormone (tri-iodo-thyronine, T_3) is well documented for its orchestration of complex homeostatic and developmental effects, from amphibian metamorphosis to mammalian brain development (Forrest et al., 1996). In humans, insufficient T_3 during development induces neurological damage and cretinism (Pitt-Rivers, 1963). In the adult brain, T_3 and its receptor, $TR\alpha 1$, are required for the full potential of cell proliferation in the SVZ (Lemkine et al., 2005).

We analyzed the molecular basis underlying the effects of the $TR\alpha 1/T_3$ complex in the SVZ. Expression of the transcription factor $TR\alpha 1$ was found in TAPs, being maintained in neuroblasts. By the use of a nonviral gene transfer method that allows transfection of the stem cell and progenitor cell populations (Lemkine et al., 2002), overexpression of $TR\alpha 1$ promoted differentiation of the transfected cells into neuroblasts and entry into the rostral migratory stream (RMS). This transfection method allowed us to follow transcriptional regulations in the SVZ. We demonstrate that the effect of $TR\alpha 1$ on commitment involves direct repression of *Sox2* by $TR\alpha 1$ binding to the *Sox2* Regulatory Region 1 (SRR1). Finally, induction of hypothyroidism in mice showed that $TR\alpha 1$ -mediated regulation of *Sox2* is T_3 dependent.

SOX2 is implicated in controlling neural progenitor maintenance (Graham et al., 2003; Pevny and Nicolis, 2010), and progenitor commitment requires *Sox2* repression to allow transcription of proneural factors (Favaro et al., 2009; Sikorska et al., 2008). Thus, the identification of factors involved in *Sox2* repression could represent a significant advance in the understanding of the cellular pathways governing stem cell to progenitor to neuroblast progression in the SVZ. However, although several pathways activating *Sox2* expression are known—e.g., CBF/NFY (Wiebe et al., 2000), Oct3/4 (Chew et al., 2005), FGF (Chew et al., 2005), EGFR (Hu et al., 2009), Shh, Gli2 (Takanaga et al., 2009), HIF (Moreno-Manzano et al., 2010), and *Ars2* (Andreu-Agullo et al., 2012)—to our knowledge, our data is the first to identify a signaling pathway favoring neurogenesis by direct repressive action on *Sox2*.

RESULTS

TR α 1 Is Expressed in TAPs and Migrating Neuroblasts

Only one T₃ binding receptor subtype, TR α 1, is expressed in the SVZ (Lemkine et al., 2005). To clarify its role, fluorescent immunohistochemistry (FIHC) using established markers for migrating neuroblasts (DCX+) and TAPs (DLX2+) was used to identify SVZ cell types expressing TR α 1 (Pastrana et al., 2011; Tavazoie et al., 2008). As shown in Figures 1A–1F, TR α 1 colocalizes with either DCX+ (Figures 1A–1C) or DLX2+ cells (Figures 1D–1F). If the large majority of DCX+ neuroblasts express TR α 1, some (about 5%) DLX2+ TAPs were negative for TR α 1 (Figures 2A–2H). It is thus probable that DLX2 expression is anterior to TR α 1, and that TR α 1 expression appears in TAPs and is maintained in neuroblasts (Figure 2I). As regards colocalization of TR α 1 and SOX2, a marker widely expressed in the SVZ niche (Tavazoie et al., 2008), we observed a strong inverse correlation in the expression of SOX2 and TR α 1, SOX2^{high} cells being TR α 1^{low} (Figures 1G–1I). SOX2^{high} cells were also DLX2^{low} (arrows in Figures 1M–1O). Similarly, DCX+ clusters of migrating neuroblasts were consistently SOX2^{low} (Figures 1J–1L and Figure S1H). Taken together, the observations suggest first, that TR α 1 expression largely colocalizes with DLX2 in TAPs, persisting after transition to the migrating neuroblast stage; and second, that these cellular transitions are accompanied by a progressive reduction in intensity of SOX2 labeling (Figures 1G–1O). To bolster this result on reciprocal levels of expression of TR α 1 and SOX2, we used TR α ^{+/0} knockin animals in which a β -gal cassette reflects TR α expression (Figures S1A–S1G). β -gal FIHC confirmed that cells expressing high levels of SOX2 had weak β -gal (TR α) signals (Figures S1D–S1F). Quantification of cells with high or low marker expression showed three populations: SOX2^{high}/TR α ^{low} or SOX2^{low}/TR α ^{high} and a few SOX2^{high} with moderate TR α expression (Figure S1G). We used GFAP/SOX2/TR α 1 triple FIHC to label type B cells (Tavazoie et al., 2008) and confirm that TR α 1 is not found in B cells (Figures S1I–S1L). Taken together, the FIHC data show that TR α 1 expression appears in TAPs and is maintained in DCX+ neuroblasts (Figures 1A–1C). These findings are summarized in Figure 2I.

TR α 1 Loss of Function in the SVZ Increases Sox2 mRNA and Numbers of SOX2-Expressing Cells

Given the strong expression of TR α 1 in TAPs and neuroblasts, we postulated that TR α 1 expression could be involved in stem cell commitment. To test this hypothesis, we examined the SVZ morphology of TR α ^{0/0} mice. Adult TR α ^{0/0} mutants displayed broader SVZs than controls (Figures 3A and 3B), with significantly increased numbers of SVZ SOX2+ cells (50.7 \pm 5.2 in controls versus 64.9 \pm 6.5 in TR α ^{0/0}, Figure 3C). To examine the acute effects of TR α 1 loss, siTR α 1 was introduced by stereotaxic injection into the lateral ventricles of adult wild-type mice. At 24 hr posttransfection of siTR α 1, qPCR showed significant downregulation of TR α 1 mRNA. This effect was specific, as TR α 2 expression was unaffected (Figure 3D). As a positive control, we confirmed that *CyclinD1* mRNA was upregulated following downregulation of TR α 1, as previously shown (Hassani et al., 2007). The modest (25%), but significant, downregulation of TR α 1 can be explained by local delivery of siTR α 1, which is diluted by dissection of the SVZ area. Nonetheless, the approach

was sufficiently efficient to reveal significant upregulation of several stem cell/TAP markers such as *Sox2*, *Nestin*, and *Msi1* mRNAs following siTR α 1 transfection (Figure 3E). TR α 1 repression is thus correlated with increased levels of neural progenitor markers.

TR α 1 Gain of Function in the SVZ Represses Sox2 Expression and Increases Numbers of DCX+ Clusters

Next the reverse experiment was performed, i.e., TR α 1 overexpression in the adult SVZ. We used a polyethylenimine (PEI)-based in vivo gene transfer method that transfects stem cells and TAP populations (Lemkine et al., 2002). Stereotaxic injection of a plasmid expressing GFP into the lateral ventricles of adult mice resulted in GFP expression mainly in Nestin+ and GFAP+ cells (Figures S2A and S2B), corresponding to NSCs and TAPS.

A schema of the experimental protocol used to overexpress TR α 1 is shown in Figure 4A. A rat TR α 1-expressing plasmid (TR α 1) was stereotaxically injected into the lateral ventricles of adult mice, which were sacrificed at either 48 hr or 4 days posttransfection. At 48 hr posttransfection, qPCR analysis confirmed increased TR α 1 mRNA levels following TR α 1 overexpression with no effect on TR α 2 levels (Figure 4B). Both *Sox2* and *CyclinD1* mRNA decreased following TR α 1 overexpression (Figure 4B).

To trace transfected cell fate, TR α 1 (or a control plasmid, with the same promoter as TR α 1) was coinjected with CMV-GFP. At 48 hr posttransfection of TR α 1, strong TR α 1 expression was found in GFP+ cells (see arrow showing GFP+, Figure 4E, and TR α 1, Figure 4G). As hypothesized, SOX2 was strongly repressed by TR α 1 overexpression (arrow, Figures 4F–4H). Quantifying the proportion of transfected cells (GFP+) expressing SOX2 after TR α 1 overexpression showed SOX2 expression in 42.8% \pm 8.9% of the transfected cells in controls, whereas TR α 1 decreased 2-fold SOX2+ cells in the transfected population (21.2% \pm 1.5%) (Figure 4C).

Because TR α 1 overexpression was correlated with downregulation of SOX2, we questioned what effect TR α 1 expression had on cell fate. Sagittal sections of brains cotransfected with TR α 1/GFP or Control/GFP were made at 4 days posttransfection and GFP FIHC was used to follow cell fate. Cells having received TR α 1 were found in DCX+ clusters at the entry to the RMS (Figures 4L–4P). In contrast, in controls, GFP transfected cells remained close to the lateral ventricle (Figures 4J and 4K). Interestingly, GFP expression was stronger in the TR α 1 compared to control-transfected cells. Because TR α 1 appears to favor a neuroblast phenotype, it is plausible that the decreased GFP expression in controls is due to dilution of plasmid in the proliferating population.

Taken together, TR α 1 loss and gain of function suggest a role of TR α 1 in *Sox2* repression and NSC commitment.

The TR α 1 Ligand, T₃, Represses Sox2 Expression in the SVZ

TR α 1 activity is modulated by its ligand, T₃. To investigate the effects of T₃ on *Sox2* expression and on NSC commitment, we used hypothyroid mice lacking T₃ (see Experimental Procedures). qPCR analysis of the SVZ of hypothyroid mice treated with saline or T₃ showed that *Sox2* expression was significantly downregulated in adults (Figures 5A and 5B) and neonatal mice (Figure S3A) by T₃ treatment.

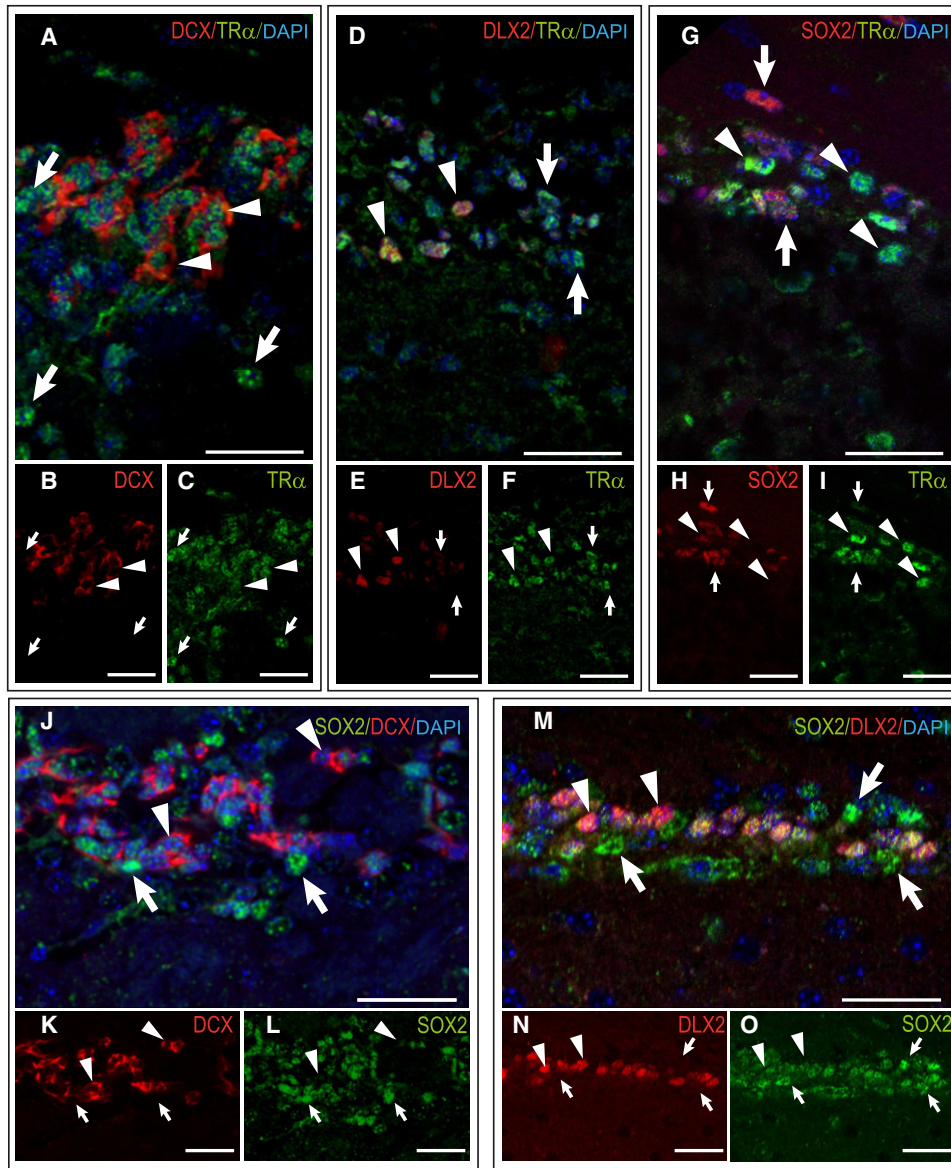


Figure 1. TR α 1 Is Expressed in Transit-Amplifying Progenitors (TAPs) and Neuroblasts of the Adult Mouse SVZ

Confocal imaging (A–O). Dorsal SVZ areas were analyzed at similar levels on coronal sections along the anterior–posterior axis (see [Experimental Procedures](#), and schema in [Figure S2](#)).

(A–C) Fluorescent Immunohistochemistry (FIHC) for TR α 1 (green) and DCX (red). DCX labels migrating neuroblasts. Arrowheads indicate TR α 1+/DCX+ clustered cells. Arrows indicate TR α 1+ cells negative for DCX. All DCX+ cells are TR α 1+.

(D–F) FIHC for TR α 1 (green) and DLX2 (red). DLX2 is expressed in TAPs in the adult SVZ. Arrowheads indicate TR α 1+/DLX2+ cells. Arrows indicate TR α 1+ cells negative for DLX2. Most DLX2+ cells are TR α 1+, but DLX2 is only expressed in a subset of TR α 1+ cells. In those cells, TR α 1 expression is positively correlated with DLX2 expression.

(G–I) FIHC for TR α 1 (green) and SOX2 (red). SOX2 is widely expressed in the adult SVZ. Cells expressing high TR α 1 levels express low or undetectable SOX2 levels (arrowheads). Cells expressing high SOX2 levels express low or no TR α 1 levels (arrows).

(J–O) FIHC for SOX2 (green) and DCX (red) (J–L) or DLX2 (red) (M–O). For imaging, we used the same parameters for SOX2 in all series. (J–L) DCX+ cells express low levels of SOX2 (arrowheads). (M–O) Cells expressing high levels of DLX2 express low or undetectable levels of SOX2 (arrowheads) whereas cells with high SOX2 levels express low or undetectable DLX2 levels (arrows).

Bars: 50 μ m. Nuclei are labeled with DAPI (blue). (See also [Figure S1](#)).

To evaluate effects of hypothyroidism on cell division and commitment in the SVZ, we performed PH3 and DLX2 immunostaining on control and hypothyroid brains. High, homogenous labeling for PH3, a mitotic cell marker, distinguishes actively

dividing, mitotic cells, whereas labeling in foci characterizes cells in interphase ([Van Hooser et al., 1998](#)). PH3-expressing cells were quantified accordingly. Compared to controls, hypothyroid mice had reduced proportions of PH3^{high}, mitotic cells and

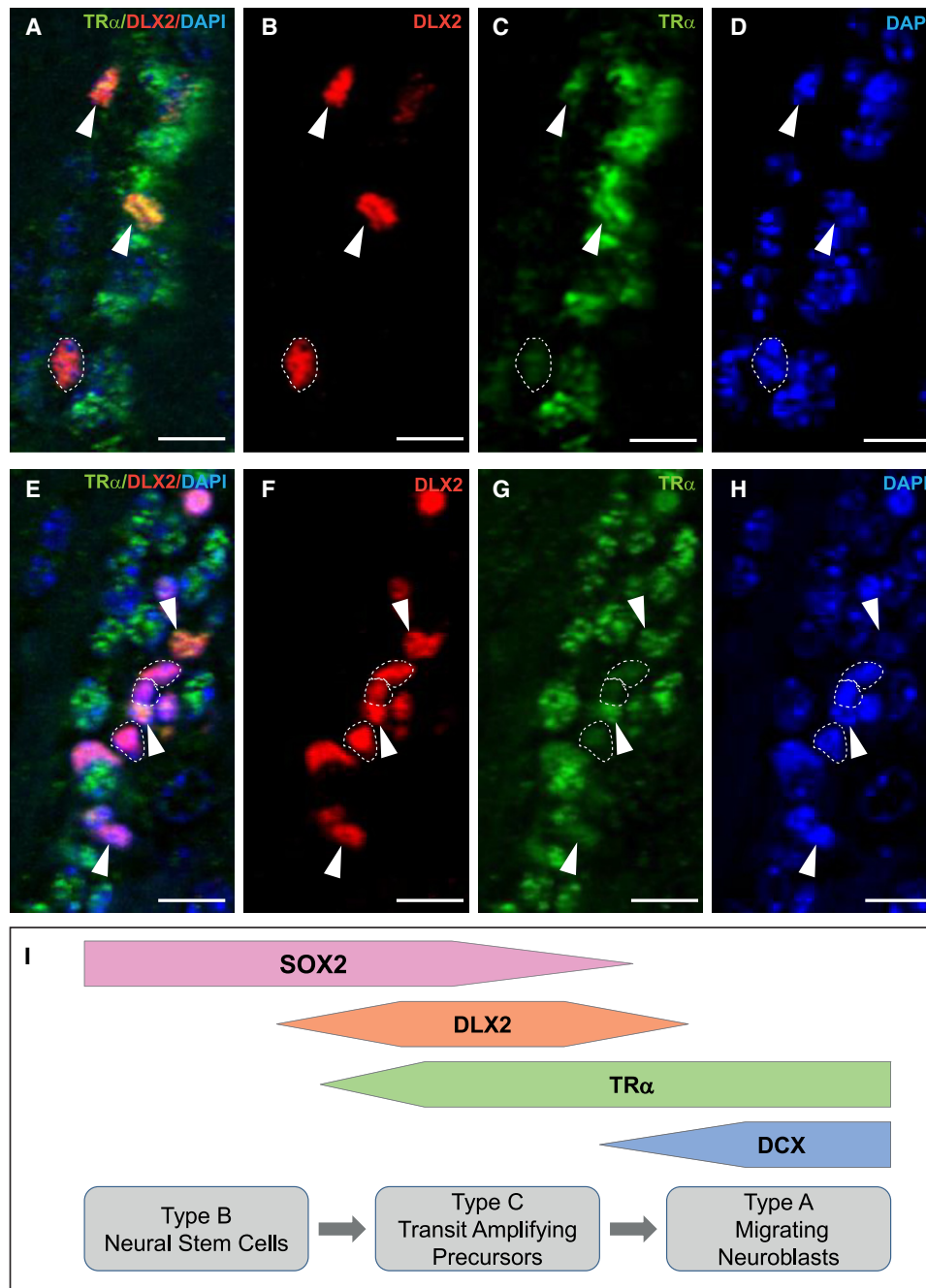


Figure 2. TR α 1 Expression Appears in TAPs in the Adult Mouse SVZ

Confocal imaging (A–H) on coronal sections. Areas for image acquisition were from dorsal SVZ (A–D) and ventral SVZ (E–H). FIHC was used to analyze TR α 1 (green) and DLX2 (red) coexpression. DLX2 is expressed in TAPs in the adult SVZ. Dotted lines circle DLX2+ cells where the TR α 1 signal did not exceed background. DAPI (blue) labels nuclei. Arrowheads indicate TR α 1+/DLX2+ cells. Diagram (I) summarizes TR α 1 expression during NSC commitment. Bars: 20 μ m.

increased numbers of cells in interphase with PH3 in foci (Figures 5C–5F). To assess effects of hypothyroidism on TAP (DLX2+ cells) commitment, DLX2+ cells were quantified. Hypothyroidism reduced the proportions of cells with high levels of DLX2 compared to controls (Figures 5G–5J). Thus, hypothyroidism increases cells in interphase within the niche, affecting the TAP population, as shown by the decrease in DLX2 bright

cells. Together these findings suggest a role for T₃ in the exit from quiescence.

The Sox2 SRR1 Enhancer Is Repressed by TR α 1/T₃

Regulation of Sox2 expression involves SRR1 and SRR2 (Figure 6A), two elements located upstream and downstream, respectively, of the Sox2 coding region (Tomioka et al., 2002).

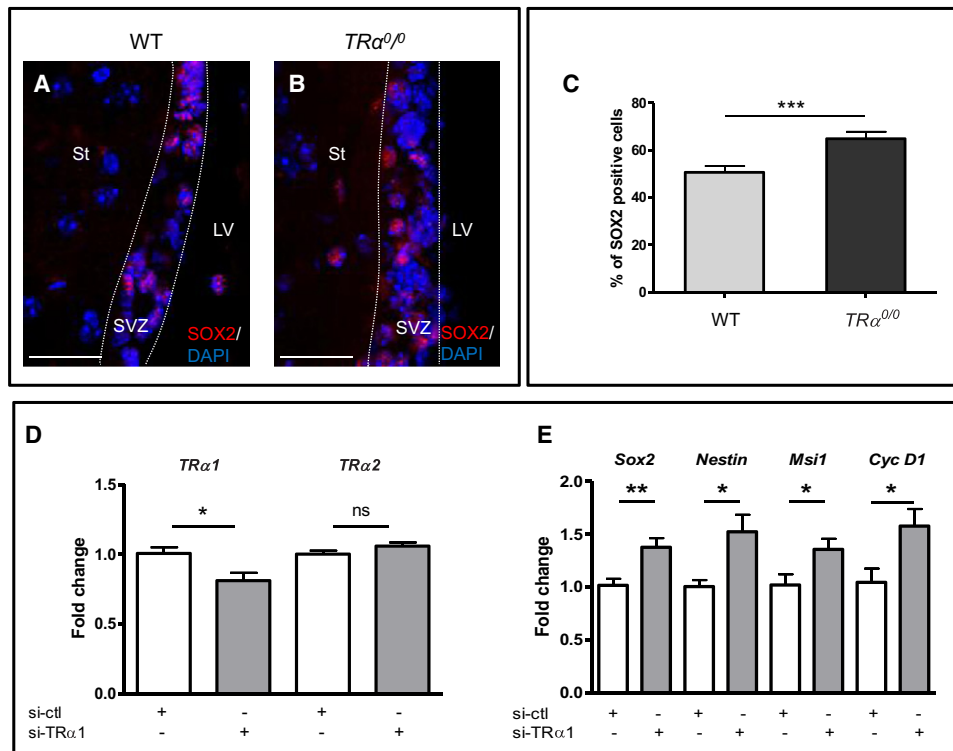


Figure 3. TR α 1 Loss of Function Increases the SOX2+ Population in Adult Mouse SVZ and Expression of Neural Stem Markers

(A and B) SOX2 FIHC (magenta) on SVZs from wild-type (WT) or TR $\alpha^{0/0}$ adult mice.

(C) The number of SOX2+ cells within the SVZ of WT and TR $\alpha^{0/0}$ mice (light gray and dark gray, respectively) were quantified (see [Experimental Procedures](#)). TR $\alpha^{0/0}$ mice had a significantly higher proportion of SOX2+ cells (around 30% more) compared to controls.

(D and E) siRNA-based transient TR α 1 knockdown in WT adult mouse SVZ. (D) siTR α 1 downregulates TR α 1, but not TR α 2, mRNA levels. (E) Transient TR α 1 knockdown upregulates Sox2 and CyclinD1. The NSC and TAP markers Nestin and Msi1 are also upregulated at 24 hr posttransfection compared to controls. Each experiment was reproduced ≥ 3 times ($n = 4$), providing similar results. Pooled data ($n \geq 12$) are shown with means \pm SEMs. Statistical analysis used nonparametric, exact permutation tests (Cytel Studio software). * $p < 0.05$, ** $p < 0.01$. Bars: 25 μ m. Nuclei are labeled with DAPI (blue). St, striatum; LV, lateral ventricle.

Both SRR1 and SRR2 show species-wide conservation, notably between human and mouse (Tomioka et al., 2002). To analyze the functional role of TR α 1 and T $_3$ in regulating Sox2 expression, we used luciferase constructs under the control of the minimal promoter region (Tomioka et al., 2002; Miyagi et al., 2006) (Figure S4B), or one of the enhancer regions, either SRR1 or SRR2 (Figure 6B). Gene transfer in newborns is faster to perform than in adult mice, so in order to build an assay with a suitably large set of biological replicates, gene transfer was done in newborns. Moreover, Sox2 expression is also regulated by T $_3$ in newborn mouse SVZ (Figure S3A). To identify the cell types transfected by PEI in the newborn mouse SVZ, we vectorized CMV-eGFP plasmids and examined cellular localization of GFP. FIHC at 24 hr posttransfection showed that transfected (GFP-expressing) cells were largely SOX2 positive (Figures S3B–S3J).

Because most SOX2^{high} cells have low TR α 1 (Figure 1G; Figures S1A–S1F, S1G, and S1J), we needed to ensure that sufficient TR α 1 was present when examining T $_3$ effects on Sox2 transcription. Thus, TR α 1 was cotransfected with SRR1-luc or SRR2-luc so that we could analyze T $_3$ -dependent regulation. Both SRR1-luc and SRR2-luc were downregulated by 20% to 30% ($p < 0.01$) in SVZ of hypothyroid mice 24 hr after T $_3$ treatment (Figure 6C, left panels). In contrast, T $_3$ treatment did not

modify transcription from the proximal promoter construct (Sox2-luc, Figure S4B), indicating that the T $_3$ -dependent element or elements regulating Sox2 might be within SRR1 and/or SRR2. To confirm the specific role of endogenous TR α 1 on activity of the two Sox2 enhancers, in vivo knockdown of endogenous TR α 1 in wild-type animals (Figure 6C) or rescue of TR α 1 in TR $\alpha^{0/0}$ mice (Figure 6D) was done. Cotransfection of shTR α 1 (Hassani et al., 2007) along with SRR1-luc or SRR2-luc doubled transcription ($p < 0.01$) from both constructs (Figure 6C, panels on right), compared to a control shRNA with the same promoter as shTR α 1 (see [Experimental Procedures](#)). This result consolidates the concept that TR α 1 represses the activity of the SRR1 and SRR2 enhancers. Furthermore, rescue of TR α 1 (by TR α 1 transfection) in the SVZ of TR $\alpha^{0/0}$ mice significantly reduced transcription from both SRR1-luc and SRR2-luc ($p < 0.05$), compared to a control plasmid with the same promoter as TR α 1, (Figure 6D), confirming that TR α 1 regulates the activity of both enhancers.

Sox2 Is a Direct Target Gene of TR α 1

TR α 1/T $_3$ -mediated repression of Sox2 could be a direct, transcriptional effect, or it could be indirect. Direct repression would involve the binding of TR α 1 to a thyroid hormone response

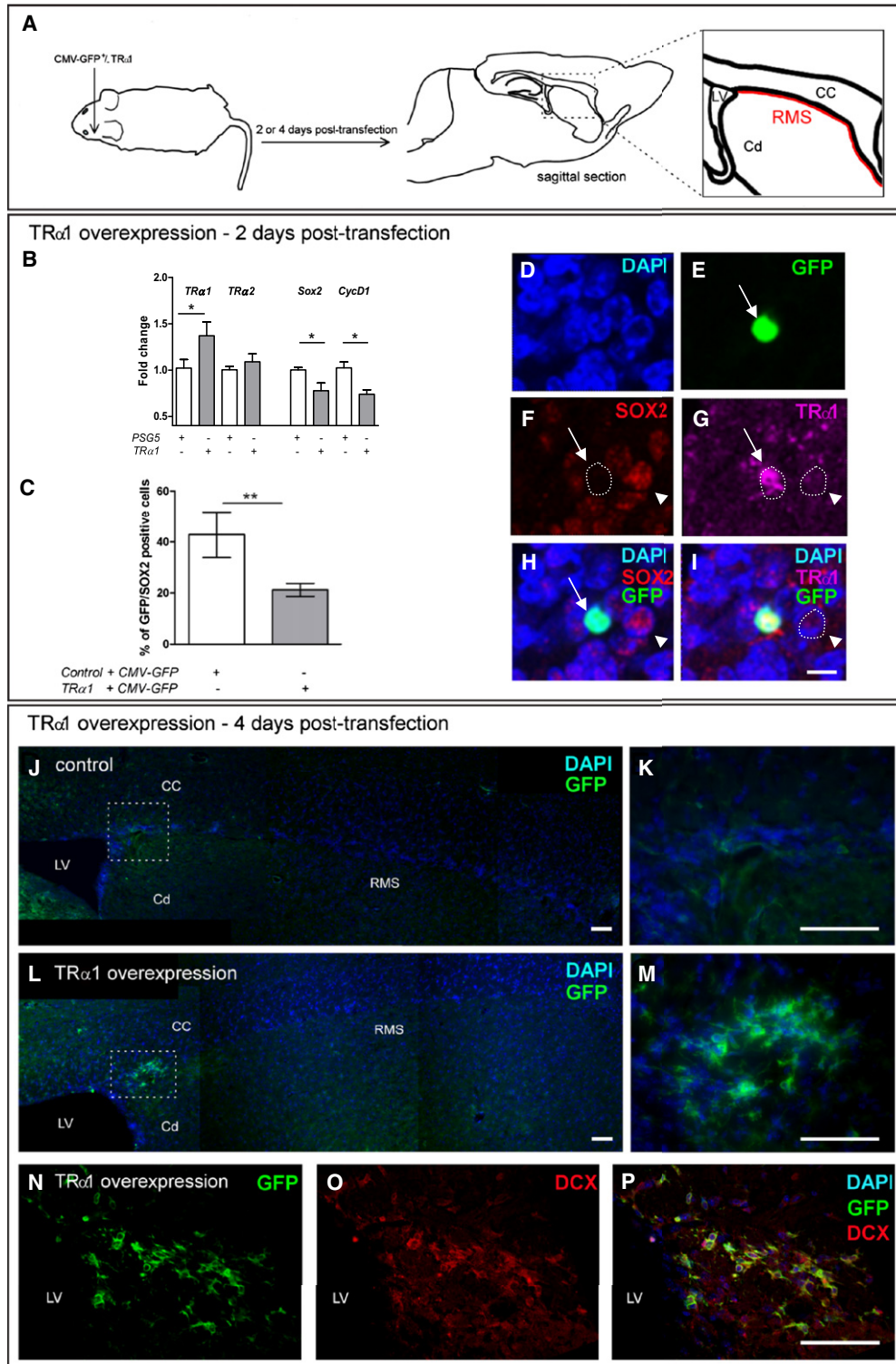


Figure 4. TR α 1 Overexpression Reduces the SOX2⁺ Population in Adult Mouse SVZ and Promotes Neuroblast Entry into the RMS

(A) Schema of experimental design: TR α 1 plasmid (TR α 1) or PSG5 vector (pControl) were mixed with CMV-eGFP and stereotactically injected into adult mouse SVZ. Two (B–I) or four (J–P) days after transfection, brains were used for qPCR (B) or for preparing coronal or sagittal sections (C–P) so as to determine the fate of the transfected cells in the lateral ventricle and RMS.

(B) qPCR analysis of SVZ dissection shows that TR α 1 transfection increases TR α 1 mRNA and decreases Sox2 and CyclinD1 mRNA levels 48 hr posttransfection. Note that overexpression of TR α 1 did not affect TR α 2 expression. $n \geq 8$ per group, means \pm SEM are given. Statistical analysis used nonparametric, exact permutation test (Cytel Studio software). * $p < 0.05$.

element (TRE) in an enhancer. In silico examination of mouse *SRR1* and *SRR2* showed two areas containing candidate negative TREs (nTREs) in *SRR1*: TRE1/2, containing two TREs, and TRE3 (Figure 7A). No candidate TRE was found in *SRR2*. To determine if T₃-dependent repression involved interaction of TR α 1 with *SRR1*, ChIP assays were performed on SVZ dissected from hypothyroid newborn mice, treated with or without T₃. TR α 1 was associated with TRE1/2 in T₃-treated, but not untreated, mice (Figure 7B). No TR α 1 binding was found on the irrelevant control regions of *Sox2* with or without T₃ (Figure 7B). To determine the functional significance of the TRE in *SRR1*, site-directed mutagenesis was used. As shown in Figure 7C, whereas T₃ significantly repressed transcription from the intact construct ($p < 0.001$), T₃ repression of *SRR1* transcription was lost on mutation of TRE1, confirming the ChIP data, which demonstrates a direct interaction of TR α 1 with *SRR1*. Further, mutation of TRE2 did not modify T₃-dependent regulation of *SRR1* (data not shown), delimiting the T₃/TR α 1 interaction to the *SRR1* TRE1 area. To bolster the physiological relevance of these results, we examined whether T₃ repression of *SRR1* was dose dependent. Significant repression was found at the lowest dose (25 ng T₃/g b.w.), with maximal repression (about 45% of control) being found between 0.25 and 2.5 μ g T₃/g b.w. (Figure S4C).

DISCUSSION

These data show that in the adult SVZ, T₃ and TR α 1, together, favor NSC commitment and progression toward a migrating neuroblast phenotype. This commitment switch correlates with T₃/TR α 1-dependent transcriptional repression of *Sox2*. To our knowledge, this study is the first description of an endogenous, hormonal signaling pathway acting on NSC commitment and migration. Clarifying how a centrally regulated, but widely distributed, endocrine signal is integrated and interpreted in a tissue- and cell-specific context is vital to understanding the physiology of stem cell niches. Hormonal control of stem cell niches has been shown in germinal stem cells of fruit flies (Gancz et al., 2011) and in shoot stem cells in plants (Zhao et al., 2010), but not in mammals.

The establishment of the role of TR α 1/T₃ in NSC progression toward commitment derives from a series of in vivo morphological and molecular studies. As recently emphasized (Pastrana et al., 2011), despite their various strengths, in vitro assays such as the neurosphere-forming assay have certain limitations, including their establishment on the basis of proliferation, which may not be limited to bona fide stem cells and thereby introduce a bias to progenitors. Another drawback is that in vitro models lose the complex cellular architecture and its intricate relation-

ships with the ventricles, cerebral spinal fluid, and the vascular system (Tavazoie et al., 2008). Other biases can arise from changes induced by nonphysiological concentrations of growth factors added for culture. Hence, our focus on in vivo, physiological approaches, including nonviral gene transfer in the SVZ (Lemkine et al., 2002, 2005) and siRNA vectorization in vivo (Hasani et al., 2007). FIHC was used to follow expression of markers within the intact SVZ, comparing wild-type mice to mice lacking TR α or euthyroid mice to hypothyroid mice.

A first element of determining how TR α 1/T₃ act on neurogenesis in the adult SVZ (Lemkine et al., 2005) was to establish the cell types expressing receptor TR α 1. TR α 1 was found in DLX2+ TAPs and DCX+ migrating neuroblasts, suggesting that its expression correlates with commitment. To test the hypothesis that TR α 1 is implicated in consolidating the TAP phenotype and promoting transition to neuroblast phenotypes, we examined the effect of targeted delivery of TR α 1 to the SVZ population. Overexpression of TR α 1 induced differentiation into DCX+ neuroblasts that entered the RMS, confirming the role of TR α 1 in favoring differentiation transitions. This finding raised the question of the molecular targets underlying TR α 1- and T₃-induced changes.

Having observed an inverse correlation between SOX2 and TR α 1 expression, and given that *Sox2* is an early marker of the NSC lineage (Bergsland et al., 2011), we hypothesized that TR α 1 expression represses *Sox2*, allowing progression of TAPs to neuroblasts. Using FIHC for SOX2 and β -gal as a TR α read-out, we noted three populations of cells (Figure S1G): Sox2^{high}/TR α ^{low}, Sox2^{low}/TR α ^{high}, and a smaller population with high levels of SOX2 and intermediate β -gal (TR α) levels. According to current thinking, the SOX2^{high} cells are probably NSCs, whereas SOX2^{low} cells represent TAPs. The smaller, third population with high SOX2 and intermediate TR α levels could represent a transition stage where SOX2 and TR α 1 are coexpressed. This observation echoes the finding that overexpression of TR α 1 repressed SOX2 expression in 50% of transfected cells (Figure 4C). An explanation for both results is that *Sox2* repression by TR α 1 requires T₃. Thus, cells that do not respond to an increase in TR α 1 by the decrease in Sox2/SOX2 probably have no available T₃, a factor that will be governed by cell-specific expression of activating and inactivating deiodinases (Williams and Bassett, 2011).

This hypothesis is supported by gain- and loss-of-function experiments showing that T₃/TR α 1 together downregulate *Sox2*. This regulation is dose dependent and direct. Mutating a negative TRE in the *SRR1* regulatory region abrogated T₃/TR α 1 repression of transcription from *SRR1*. Further, ChIP analysis showed T₃-dependent association of TR α 1 with *SRR1*. T₃ also downregulated *SRR2*. This area does not contain

(C) Quantification of SOX2+ cells following transfection of TR α 1 or pControl. Percentages of double-labeled SOX2+ and GFP+ cells decrease following TR α 1 overexpression. The experiment was repeated three times (n = 4), providing similar results. Values represent means \pm SEM. ** $p < 0.01$ by exact nonparametric permutation test for multiple samples (Cytel Studio software).

(D–I) FIHC on coronal sections following transfection of TR α 1/CMV-eGFP (pControl/CMV-eGFP was used for controls). Arrows in (E)–(H) indicate a GFP+ (green)/TR α 1+ (magenta) cell (E and G) that is negative for SOX2 (F). Arrowheads in (F)–(I) indicate a SOX2+ cell that is negative for GFP/TR α 1.

(J–P) FIHC on sagittal sections of control or TR α 1-transfected brains. (J and K) In controls, cells transfected with pControl (GFP+, green) are limited to the SVZ. (K) and (M) are high magnifications of the boxed areas (dotted lines) in (J) and (L), respectively. (L–P) In a TR α 1-transfected brain, a group of overexpressing TR α 1 cells (GFP+ cells in green) is observed entering the RMS. (N–P) The group of TR α 1/CMV-eGFP-expressing cells in (M) also express the neuroblast marker DCX (red) (O).

Representative brains are shown, n = 4 per condition. Bars: (D–I) = 10 μ m; (J–P) = 50 μ m. (See also Figure S2.)

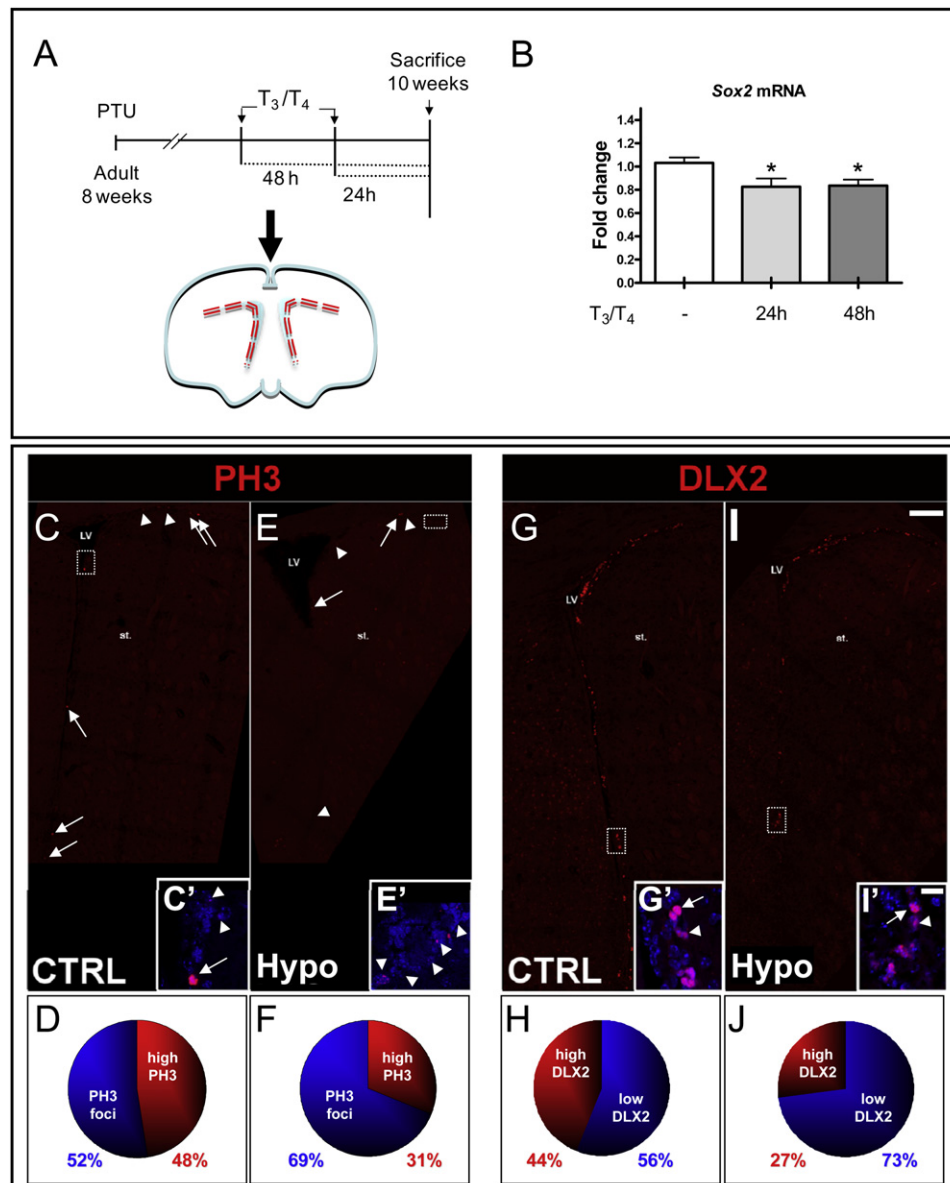


Figure 5. T₃ Represses Sox2 Expression and Modulates Cellular Proliferation in the SVZ, Affecting the TAP Population

(A) Schema of experimental design. SVZ of hypothyroid adult mouse brains were dissected 24 or 48 hr post T₃/T₄ treatment (controls received NaCl). (B) Sox2 mRNA quantified by qPCR was normalized against *Gapdh* using the DDCT method. Sox2 levels are given as a function of control levels. Pooled data from three experiments are given, means \pm SEM (n \geq 12). Statistical analysis used nonparametric, exact permutation test (Cytel Studio software). *p < 0.05. (See also Figure S3).

(C–J) FIHC for PH3 (C–E) and DLX2 (G–I) on coronal sections of control (CTRL) (C and G) and hypothyroid (Hypo) (E and I) mouse brain. Dotted squares in (C) and (E) denote regions magnified in insets (C' and E') where PH3 is in red and nuclei are in blue (DAPI). Cells in G2 phase have punctuated PH3 staining (see arrowheads, C, C', E, and E'), whereas cells in M phase have dense uniform PH3 staining (see arrows, C, C', and E). As shown in (D) and (F), hypothyroidism is associated with decreased proportion of high PH3+ cells, compared to controls. Dotted squares (in G and I) denote regions magnified in insets (G' and I') in which DLX2 is in red and nuclei are in blue (DAPI). Two populations of DLX2+ cells are observed: DLX2-high+ cells (see arrows, G' and I') and DLX2-low+ cells (see arrowheads in G' and I'). Hypothyroidism is associated with a decrease of the proportion of high DLX2+ cells compared to controls (H versus J). Bars: I = 100 μ m; I' = 10 μ m.

a consensus TRE, suggesting indirect regulation of SRR2 by T₃. SRR2 contains a Sox2/Oct4 binding box activated by SOX2 itself (Tomioka et al., 2002). Thus, SRR2 repression by T₃ could entail T₃-mediated decrease of SOX2 protein. The findings that T₃/TR α 1 promote commitment and repress Sox2 are in accor-

dance with demonstrations that Sox2 repression correlates with neural differentiation in vitro (Cimadamore et al., 2011; Bylund et al., 2003).

Interestingly, our data indicate that TR α 1 knockdown with siRNA increases not only Sox2 levels but also *CyclinD1* mRNA

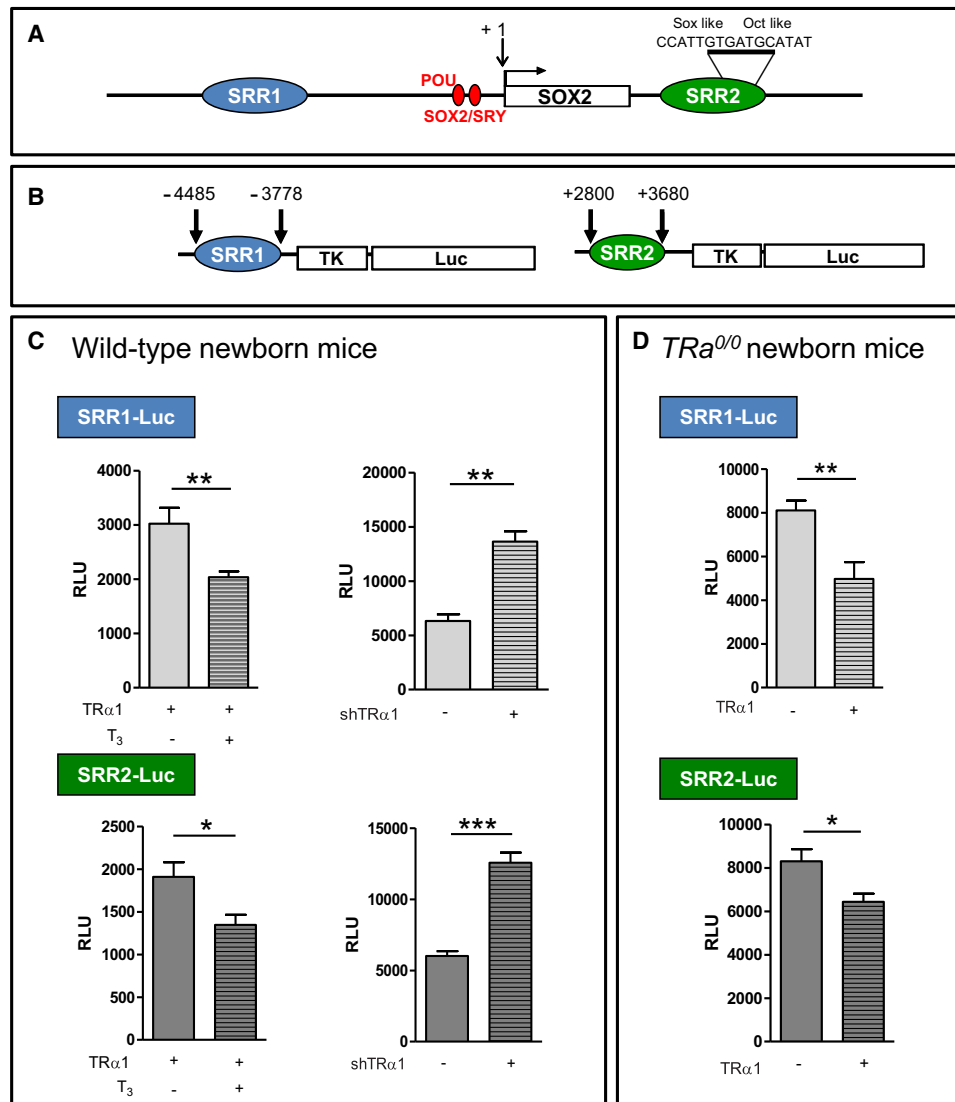


Figure 6. Transcription from Sox2 Regulatory Regions SRR1 and SRR2 Is Repressed by T₃ and TR α 1

(A) Schema of Sox2 and its characterized regulatory regions: Sox2 minimal promoter, SRR1, and SRR2.

(B) SRR1 (-4485 to -3778 from ATG) and SRR2 (+2800 to +3680 from ATG) sequences were cloned into reporter plasmids: SRR1-Luc and SRR2-Luc, respectively (see Experimental Procedures).

(C) Transcriptional activity from SRR1-Luc (upper panel) or SRR2-Luc (lower panel) \pm T₃ (left) or TR α 1 knockdown (right). Left panel: stereotaxic injections of SRR1-Luc or SRR2-Luc cotransfected with TR α 1 into lateral ventricles of hypothyroid wild-type newborn mice. In each case, mice received T₃ or saline. Both SRR1-Luc and SRR2-Luc are significantly downregulated by T₃. Right panel: SRR1-Luc or SRR2-Luc was cotransfected with shTR α 1-expressing vectors in the lateral ventricles of euthyroid wild-type newborn mice. shTR α 1 significantly increases SRR1-Luc and SRR2-Luc activity as compared to control-plasmid-injected brains.

(D) In TR α ^{0/0} homozygous mice, cotransfection of TR α 1 represses transcription from SRR1-Luc and SRR2-Luc.

In all cases, representative experiments are shown (means \pm SEMs). Statistical analysis used nonparametric, exact permutation test (Cytel Studio software). *p < 0.05, **p < 0.01, ***p < 0.001. Each experiment was performed in triplicate (n = 10 wild-type; n = 6, TR α ^{0/0}). (See also Figure S4.)

levels. Previous data showed repression of *CyclinD1* expression by TR α 1/T₃ in the neonatal SVZ (Hassani et al., 2007). Lange et al. (2009) have shown that *CyclinD1* downregulation in the SVZ lengthens the cell cycle, which is a necessary prerequisite to promote neuronal differentiation. Taking these results together, we propose that the double-pronged repression of Sox2 and *CyclinD1* by TR α 1/T₃ promotes differentiation of progenitors to a more committed phenotype.

These demonstrations of the role of TR α 1 in adult neurogenesis lead to consideration of the brain phenotypes of mice lacking TR α (TR α ^{0/0} mice) or bearing TR α mutants. Kapoor et al. (2010) examined hippocampal neurogenesis in mice with a TR α 1 mutant that acts as an apo-receptor causing receptor-mediated brain hypothyroidism. These mice show reduced hippocampal neurogenesis, memory impairment, depressive behavior, and anxiety (Venero et al., 2005; Pilhatsch et al., 2010). These

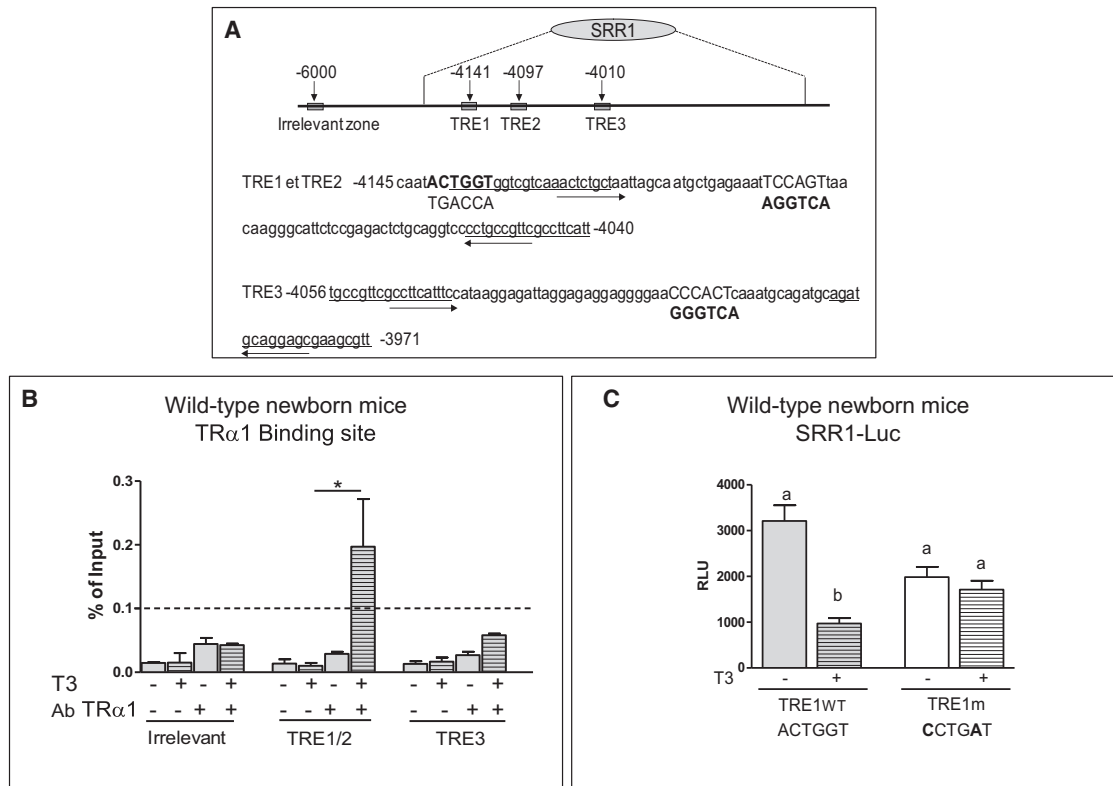


Figure 7. Direct Interaction with, and Repression of, SRR1 Activity by TR α 1 and T₃

(A) Schema of positions and putative TRE sequences in mouse SRR1. Three candidate TREs are shown (capital letters). Primers (underlined) used in PCR for detection of TREs in the ChIPs products encompassed TRE1 and 2 together or TRE3 alone.

(B) qPCR quantification of ChIP assays on SVZ from hypothyroid newborn mice treated with or without T₃ for 6 hr. Samples were immunoprecipitated with TR α 1 antibody and amplified with Sox2 TRE1/2, TRE3, or irrelevant control primers. For negative controls, samples were processed without antibody. Data are represented as percentage of input (sonicated DNA used for ChIP). Threshold value for a positive signal was set at 0.1% of input (dashed line). Experiments were run at least twice, providing similar results. Pooled data are given, means \pm SEM, **p* < 0.05.

(C) Transcriptional repression of SRR1 by T₃ requires an intact TRE1. Site-directed mutagenesis was used to mutate TRE1. Transcription from the wild-type (left panel) and mutated constructs (right panel) was compared with saline (–) or T₃ (+). A representative experiment, reproduced three times, is shown (means \pm SEM, *n* = 10 per group). Different letters indicate significant differences between groups (*p* < 0.001).

findings can be linked first, to the mood disorders and cognitive dysfunction seen in hypothyroid humans (Samuels, 2008), and second, to the potential implication of impaired adult neurogenesis in depression (David et al., 2009; Lledo, 2009).

A major question arising now is how availability of the active TR ligand, T₃, affects homeostasis and plasticity of the adult neurogenic niche. Induction of hypothyroidism in adults increased the proportion of SVZ cells held in interphase, G₂, decreasing the proportion of cells with high PH3 labeling. This result echoes the demonstration by Lemkine et al. (2005) using other markers (BrdU and Ki67) and showing that hypothyroidism blocks, and T₃ reactivates, cell cycling in the adult SVZ. The additional information provided here is that hypothyroidism leads to an increase of cells in interphase, suggesting a potential role of T₃ in the exit from quiescence. This hypothesis is corroborated by the decrease of DLX2+, highly proliferative TAPs, in response to T₃ deficiency.

In turn, these observations raise questions of how T₃ availability is determined spatiotemporally in the SVZ and the pathological consequences of changes in availability, i.e., T₃ excess or absence. T₃ availability is determined by deiodinase activity (Wil-

liams and Bassett, 2011). In the brain T₃ production from the pro-hormone thyroxine (T₄) is catalyzed by deiodinase type 2 (D2), whereas deiodinase type 3 (D3) promotes degradation of T₄ or T₃ into inactive forms (Köhrle, 2000). Future studies will be needed to clarify physiological control of T₃ production, use, and degradation in neurogenic zones. Notably, it is important to determine which cells in the SVZ express each of the deiodinases and whether these same cells also express membrane transporters for TH (Friesema et al., 2006).

T₃ availability and stemness are linked to pathology, notably tumorigenesis. D3 expression increases in certain cancers (Dentice et al., 2009). Oppel et al. (2011) found Sox2 in glioma cells, where its expression is associated with a less-differentiated phenotype. Given the role of T₃/TR α 1 signaling in not only NSCs, but also intestinal stem cells (Kress et al., 2009, 2010), such findings argue for analysis of whether T₃ signaling and TR α 1-controlled gene networks are involved in adult stem cell transitions to cancer stem cells.

In conclusion, this work underlines how an endocrine signal, T₃, by repressing Sox2 expression, acts as a switch to activate

NSC commitment. The absence of TH signaling limits the generation of neuroblasts, leading to an accumulation of Sox2+ progenitors. Synchronous repression of Sox2, *CyclinD1* (Hassani et al., 2007), and *c-myc* (Lemkine et al., 2005) will facilitate commitment and differentiation of the progenitor cell population. This demonstration of the role of T₃ in controlling stemness opens up novel research perspectives, ranging from basic issues such as understanding physiological controls governing the amount of T₃ available in stem cell niches to potential applications in treatment of pathological conditions.

EXPERIMENTAL PROCEDURES

Animals

All animal studies were conducted according to the principles and procedures described in Guidelines for Care and Use of Experimental Animals.

TR α ^{0/0} mice (from ENS, Lyon, France, Gauthier et al., 2001), lacking TR α 1, TR α 2, TR $\Delta\alpha$ 1, and TR $\Delta\alpha$ 2, were maintained on a 129/Sv strain. The DNA construct for gene targeting was engineered to associate disruption of *Thra* with an in-frame insertion of the LacZ gene. Wild-type 129/Sv mice were from Charles River Laboratories (L'Arbresle, France). Only male mice were used for adult studies.

PTU and TH Treatments

To induce hypothyroidism in newborn mice, pregnant female OF1 mice (Janvier, Le Genest St. Isle, France) were given iodine-deficient food containing 6-n-propyl-2-thiouracil (PTU) (at 0.15%, from Harlan Teklad, Madison, WI) and PTU (0.5 g/l) diluted in drinking water 7 days before the predicted day of birth. Hypothyroidism in adult mice was induced with iodine-deficient food (PTU: 0.15%) and PTU in drinking water (0.5 g/l) for 2 weeks. To evaluate TH effects, T₃ (2.5 mg/g b.w.) diluted in physiological solution was injected subcutaneously in newborn mice, or T₃/T₄ (0.3/0.012 μ g/g b.w.) was given intraperitoneally in adults along with T₄ in drinking water (12 μ g/ml). Controls received NaCl (0.9%) and tap water.

Plasmids

The murine Sox2 regulatory regions 1 and 2 (SRR1 and SRR2 [−4485/−3778 and +2072/+3681, respectively]), subcloned into Tk-Luc reporter plasmid (Stratagene) (Tomioaka et al. (2002), were a kind gift of Dr. A. Okuda (Saitama, Japan). Two putative TREs present in SRR1 were mutated in the SRR1-Luc construction using the QuikChange II XL Site-directed Mutagenesis kit (Stratagene, La Jolla, CA).

The TR α 1 expression vector containing the main domain of rat TR α 1 was subcloned into pSG5 (Stratagene) (Guissouma et al., 2002). The plasmid driving transcription of a shRNA against TR α 1 from a CMV-H1 hybrid promoter has been described (Hassani et al., 2007). The GFP expression plasmid contains the GFP coding sequence under a CMV promoter (Clontech, Palo Alto, CA).

Formulation of Polyethylenimine/DNA Complexes, and Stereotaxic Injections

Endotoxin-free plasmid DNA (Genomed, Research Triangle Park, NC) was diluted in 5% glucose and complexed with in vivo-jetPEI (Polyplus transfection; ratio of 6 PEI nitrogen per DNA phosphate, as described in Goula et al., 1998). Stereotaxic injection into the lateral ventricles of newborn mice brains was as described (Hassani et al., 2005) using a single injection (1 μ g DNA in 2 μ l) per lateral ventricle of newborn mice. Mice were sacrificed and the SVZ was dissected 24 hr later. Luciferase assays were done on brain homogenates. Ten animals were injected per group, and each SVZ was analyzed separately for luciferase activity (i.e., n = 20 SVZ per group).

Adult OF1 mice (8 weeks old, Janvier) were anaesthetized with V-tranquile (2 mg/kg b.w.; Imalgen, Ceva Santé Animal) followed by ketamine (100 mg/kg b.w.; Imalgen, Merial). The animals were transfected by unilateral stereotaxic injection (5 μ l) into the right ventricle (0.2 mm posterior to bregma line, 1.1 mm lateral, and 2.2 mm deep from the pial surface; see Lemkine et al., 2005 for details). Analgesia treatment was performed using Meloxicam (formulated as Metacam from Boehringer Ingelheim).

Formulation of siRNA Complexes

siRNA against pGL2 (for control group) or TR α 1 (siTR α 1) was synthesized by QIAGEN (for sequence, see Hassani et al., 2007). siRNA (24 pmol per animal) was diluted in glucose (5%) and complexed with monocationic lipid (INTERFERin™ IC10 from Polyplus-transfection) at a ratio of 15 monocationic lipid nitrogens per RNA phosphate. Stereotaxic injections were performed as above.

FIHC

Mice were deeply anesthetized with Pentobarbital (130 mg/kg, Sanofi) then perfused (3 ml/min) with saline solution (0.9%). Brains were dissected and fixed in paraformaldehyde (2%) in PBS (0.1 M, pH 7.4) at 4°C overnight (O/N), cryoprotected in sucrose (30%), embedded in OCT, frozen, and stored (−80°C). FIHC used cryostat coronal or sagittal sections (30 μ m). Floating brain sections were washed (3 × 10 min) with PBS in multiwell plates. Blocking was done by incubation (1 hr) in normal donkey serum (10%). Slides were incubated O/N at 4°C with the following primary antibodies: rabbit anti-SOX2 (Chemicon, 1:200) or goat anti-SOX2 (Santa Cruz, 1:200). Rabbit TR α 1 antibody was from Rockland (1:200 O/N at 4°C). Goat anti- β -galactosidase antibody (Cappel, 1:300) was incubated for 1 hr at room temperature after two glycine pretreatments (0.1M, 5 min). Rabbit anti-PH3 (Millipore, 1/300); guinea pig anti-DCX (Millipore, 1:300), guinea pig anti-DLX2 (Kuwajima et al., 2006; 1:3,000) and mouse anti-GFP (Roche, 1:300) was used. Fluorescent secondary antibodies (Invitrogen) were as follows: Alexa Fluor 647 nm donkey anti-rabbit (1:500), Alexa Fluor 594 nm donkey-anti-guinea pig (1:500), Alexa Fluor 488 nm donkey anti-rabbit (1:500), and Alexa Fluor 594 nm donkey anti-goat (1: 500) for 2 hr at room temperature. Finally, brain sections were mounted onto SuperFrost/Plus glass slides (Fisher) and air-dried before being mounted with ProLong Gold antifade reagent with the nuclear marker DAPI (Invitrogen). For imaging, we used a LSM 710 confocal microscope and ApoTome system (Carl Zeiss, Thornwood, NY).

Signal Intensity Quantification

Cell counts (PH3-, DLX2-, and SOX2+ cells) were done on coronal (0.7–1.2 anterior to bregma) or sagittal (30 μ m) sections and carried out double-blindly by two observers. For each marker, all positive cells in SVZ were counted on three consecutive slides per brain (n = 3 per group).

DLX2+ cells were sorted into two populations based upon the level of their fluorescence intensity. Regions of interest (ROI) were defined and analyzed using FIJI software (ImageJA 1.43h, <http://rsb.info.nih.gov/ij/>). Gray level threshold was stabilized at 225. The ratio of each subpopulation (DLX2-high or -low; PH3 punctuate or PH3 high) is reported as a function of all the DLX2- or PH3+ cells, respectively, counted in the SVZ.

In Vivo ChIP

Hypothyroid pups (1 day postnatal) were treated with T₃ or vehicle and sacrificed 6 hr later. SVZs were dissected and six SVZs were pooled, yielding about 40 mg of tissue. DNA-protein complexes were isolated as described (Decherf et al., 2010). Samples were fixed in 1% formaldehyde solution and sonicated. Control and T₃-treated samples were used for ChIP with anti-TR α 1 antibodies (Thermo Scientific, Rockford, USA) or without antibody (negative control). Precipitated DNA fragments were purified. DNA from ChIP with or without antibody and from input sample (sonicated DNA not included in the ChIP reaction) was used for real-time PCR using Applied Biosystems 7300 real-time PCR System and Power SYBR Green PCR Master Mix from Applied Biosystems. Several sets of primers were used for Sox2 (see Figure 7). The PCR reaction (25 μ l) was started by a step of 10 min at 95°C followed by 35 cycles of 15 s, 95°C, 1 min 60°C. Quantifications used data from the qPCR. Data are presented as percentage of input (see above). Threshold value for positive signals was set at 0.1% of input (dashedline on the histograms).

qPCR

SVZs of pups and adults were dissected under binocular microscope, snap-frozen in liquid nitrogen, and stored (−80°C) until processed. Total RNA concentrations were measured and RNAs were stored in Tris 10 mM/EDTA 0.1 mM (pH 7.4) at −80°C. To quantify mRNAs, 1 μ g of total RNA was reverse-transcribed using high capacity cDNA Reverse Transcription kit (Applied Biosystems,

Courtaboeuf, France). Control reactions without reverse transcriptase were done in parallel. Primers from Taqman Gene expression assays were used for the mRNA detection of the following: *Sox2* (Mm03053810_s1), *cyclinD1* (Mm00432360_m1), *Nestin* (Mm01223404_g1), *Msi1* (Mm00485224_m1), *Cspg4* (also called NG2; Mm00507256_m1), *Ascl1* (also called Mash1; Mm03058063_m1), *elavl4* (also called *hud*; Mm00516018_m1), and control assays (*Gapdh*; Mm99999915_g1). Primers for TR α 1 and TR α 2 were designed in the laboratory (Hassani et al., 2007) and purchased from MWG Biotech (Roissy CDG, France).

Direct detection of the PCR product was monitored by measuring the increase in fluorescence generated by the TaqMan probe (*Sox2*, *CyclinD1*, *Nestin*, *Msi1*, *NG2*, *Mash1*, *elavl4*, or *Gapdh*) or by the binding of SYBR Green to dsDNA (TR α 1 or TR α 2) as described previously by Decherf et al. (2010).

Statistical Analysis

All experiments had $n < 30$; therefore, statistical analysis used nonparametric, exact permutation tests (StatXact9, Cytel Studio software). This analysis carries out permutations on exact values and is more powerful than the Mann Whitney test. Note that for a population with normality, the median is equal to the mean. Statistical differences were analyzed with appropriate tests, indicated in figure legends, to compare control and treated group. $p < 0.05$ was considered significant ($*p < 0.05$; $**p < 0.01$; $***p < 0.001$).

SUPPLEMENTAL INFORMATION

Supplemental Information for this article includes four figures and can be found with this article online at doi:10.1016/j.stem.2012.04.008.

ACKNOWLEDGMENTS

This work was supported by the Centre National de la Recherche Scientifique (CNRS), the Museum National d'Histoire Naturelle (MNHN), the Association Française contre les Myopathies (AFM), European Union contracts "Crescendo" and "Switchbox," and the French ANRs "Signator" and "Thrast." A.L.-J. received a Ph.D. grant from the Association nationale de la Recherche et technologie (ANRT) and Polyplus-transfection S.A. under CIFRE convention No. 251/2007. We thank P. Bilesimo, L. Sachs, and M.S. Clerget-Froidevaux for advice on experimental techniques; Gladys Alfama for technical assistance; and G. Levi for insightful comments. M. Gèze and the Plateforme d'Imagerie du MNHN provided excellent imaging advice. The excellent animal care by Stéphane Sosinsky, Philippe Durand, and Fabien Uridat is gratefully acknowledged. J.P. acts as a consultant for ReNeuron. The authors declare that there is no conflict of interest that would prejudice the impartiality of this scientific work.

Received: December 30, 2010

Revised: January 12, 2012

Accepted: April 9, 2012

Published: May 3, 2012

REFERENCES

Andreu-Agullo, C., Maurin, T., Thompson, C.B., and Lai, E.C. (2012). *Ars2* maintains neural stem-cell identity through direct transcriptional activation of *Sox2*. *Nature* 481, 195–198.

Bergsland, M., Ramsköld, D., Zauter, C., Klum, S., Sandberg, R., and Muhr, J. (2011). Sequentially acting Sox transcription factors in neural lineage development. *Genes Dev.* 25, 2453–2464.

Bylund, M., Andersson, E., Novitsch, B.G., and Muhr, J. (2003). Vertebrate neurogenesis is counteracted by Sox1–3 activity. *Nat. Neurosci.* 6, 1162–1168.

Chew, J.L., Loh, Y.H., Zhang, W., Chen, X., Tam, W.L., Yeap, L.S., Li, P., Ang, Y.S., Lim, B., Robson, P., and Ng, H.H. (2005). Reciprocal transcriptional regulation of Pou5f1 and Sox2 via the Oct4/Sox2 complex in embryonic stem cells. *Mol. Cell Biol.* 25, 6031–6046.

Cimadamore, F., Fishwick, K., Giusto, E., Gnedeva, K., Cattarossi, G., Miller, A., Pluchino, S., Brill, L.M., Bronner-Fraser, M., and Terskikh, A.V. (2011).

Human ESC-derived neural crest model reveals a key role for SOX2 in sensory neurogenesis. *Cell Stem Cell* 8, 538–551.

David, D.J., Samuels, B.A., Rainer, Q., Wang, J.W., Marsteller, D., Mendez, I., Drew, M., Craig, D.A., Guiard, B.P., Guilloux, J.P., et al. (2009). Neurogenesis-dependent and -independent effects of fluoxetine in an animal model of anxiety/depression. *Neuron* 62, 479–493.

Decherf, S., Seugnet, I., Kouidhi, S., Lopez-Juarez, A., Clerget-Froidevaux, M.S., and Demeneix, B.A. (2010). Thyroid hormone exerts negative feedback on hypothalamic type 4 melanocortin receptor expression. *Proc. Natl. Acad. Sci. USA* 107, 4471–4476.

Dentice, M., Ambrosio, R., and Salvatore, D. (2009). Role of type 3 deiodinase in cancer. *Expert Opin. Ther. Targets* 13, 1363–1373.

Doetsch, F., García-Verdugo, J.M., and Alvarez-Buylla, A. (1999). Regeneration of a germinal layer in the adult mammalian brain. *Proc. Natl. Acad. Sci. USA* 96, 11619–11624.

Doetsch, F., Petreanu, L., Caille, I., Garcia-Verdugo, J.M., and Alvarez-Buylla, A. (2002). EGF converts transit-amplifying neurogenic precursors in the adult brain into multipotent stem cells. *Neuron* 36, 1021–1034.

Favaro, R., Valotta, M., Ferri, A.L., Latorre, E., Mariani, J., Giachino, C., Lancini, C., Tosetti, V., Ottolenghi, S., Taylor, V., and Nicolis, S.K. (2009). Hippocampal development and neural stem cell maintenance require Sox2-dependent regulation of Shh. *Nat. Neurosci.* 12, 1248–1256.

Forrest, D., Golarai, G., Connor, J., and Curran, T. (1996). Genetic analysis of thyroid hormone receptors in development and disease. *Recent Prog. Horm. Res.* 51, 1–22.

Friesema, E.C., Kuiper, G.G., Jansen, J., Visser, T.J., and Kester, M.H. (2006). Thyroid hormone transport by the human monocarboxylate transporter 8 and its rate-limiting role in intracellular metabolism. *Mol. Endocrinol.* 20, 2761–2772.

Gancz, D., Lengil, T., and Gilboa, L. (2011). Coordinated regulation of niche and stem cell precursors by hormonal signaling. *PLoS Biol.* 9, e1001202.

Gauthier, K., Plateroti, M., Harvey, C.B., Williams, G.R., Weiss, R.E., Refetoff, S., Willott, J.F., Sundin, V., Roux, J.P., Malaval, L., et al. (2001). Genetic analysis reveals different functions for the products of the thyroid hormone receptor alpha locus. *Mol. Cell Biol.* 21, 4748–4760.

Goula, D., Benoist, C., Mantero, S., Merlo, G., Levi, G., and Demeneix, B.A. (1998). Polyethylenimine-based intravenous delivery of transgenes to mouse lung. *Gene Ther.* 5, 1291–1295.

Graham, V., Khudyakov, J., Ellis, P., and Pevny, L. (2003). SOX2 functions to maintain neural progenitor identity. *Neuron* 39, 749–765.

Guissouma, H., Dupré, S.M., Becker, N., Jeannin, E., Seugnet, I., Desvergne, B., and Demeneix, B.A. (2002). Feedback on hypothalamic TRH transcription is dependent on thyroid hormone receptor N terminus. *Mol. Endocrinol.* 16, 1652–1666.

Hassani, Z., Lemkine, G.F., Erbacher, P., Palmier, K., Alfama, G., Giovannangeli, C., Behr, J.P., and Demeneix, B.A. (2005). Lipid-mediated siRNA delivery down-regulates exogenous gene expression in the mouse brain at picomolar levels. *J. Gene Med.* 7, 198–207.

Hassani, Z., François, J.C., Alfama, G., Dubois, G.M., Paris, M., Giovannangeli, C., and Demeneix, B.A. (2007). A hybrid CMV-H1 construct improves efficiency of PEI-delivered shRNA in the mouse brain. *Nucleic Acids Res.* 35, e65.

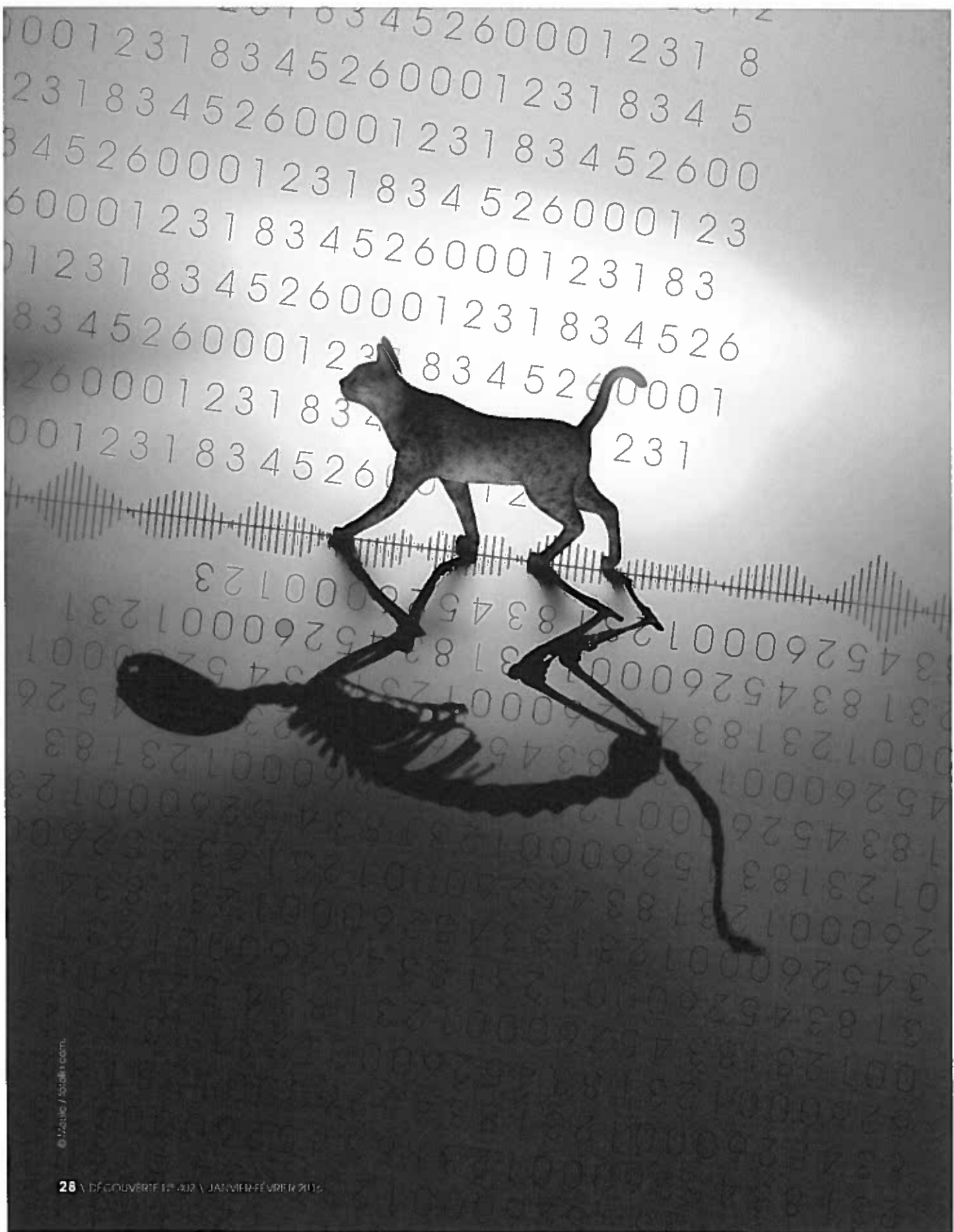
Hu, Q., Zhang, L., Wen, J., Wang, S., Li, M., Feng, R., Yang, X., and Li, L. (2009). The EGF Receptor-Sox2-Egf Receptor Feed-Back Loop Positively Regulates the Self-Renewal of Neural Precursor Cells. *Stem Cells* 28, 279–286.

Kapoor, R., van Hogerlinden, M., Wallis, K., Ghosh, H., Nordstrom, K., Vennstrom, B., and Vaidya, V.A. (2010). Unliganded thyroid hormone receptor alpha1 impairs adult hippocampal neurogenesis. *FASEB J.* 24, 4793–4805.

Köhrle, J. (2000). The selenoenzyme family of deiodinase isozymes controls local thyroid hormone availability. *Rev. Endocr. Metab. Disord.* 1, 49–58.

Kress, E., Samarut, J., and Plateroti, M. (2009). Thyroid hormones and the control of cell proliferation or cell differentiation: paradox or duality? *Mol. Cell. Endocrinol.* 313, 36–49.

- Kress, E., Skah, S., Sirakov, M., Nadjar, J., Gadot, N., Scoazec, J.Y., Samarut, J., and Plateroti, M. (2010). Cooperation between the thyroid hormone receptor TR α 1 and the WNT pathway in the induction of intestinal tumorigenesis. *Gastroenterology* 138, 1863–1874.
- Kuwajima, T., Nishimura, I., and Yoshikawa, K. (2006). Necdin promotes GABAergic neuron differentiation in cooperation with Dlx homeodomain proteins. *J. Neurosci.* 26, 5383–5392.
- Lange, C., Huttner, W.B., and Calegari, F. (2009). Cdk4/cyclinD1 overexpression in neural stem cells shortens G1, delays neurogenesis, and promotes the generation and expansion of basal progenitors. *Cell Stem Cell* 5, 320–331.
- Lemkine, G.F., Mantero, S., Migné, C., Raji, A., Goula, D., Normandie, P., Levi, G., and Demeneix, B.A. (2002). Preferential transfection of adult mouse neural stem cells and their immediate progeny in vivo with polyethylenimine. *Mol. Cell. Neurosci.* 19, 165–174.
- Lemkine, G.F., Raj, A., Alfama, G., Turque, N., Hassani, Z., Alegria-Prévot, O., Samarut, J., Levi, G., and Demeneix, B.A. (2005). Adult neural stem cell cycling in vivo requires thyroid hormone and its alpha receptor. *FASEB J.* 19, 863–865.
- Lledo, P.M. (2009). Dissecting the pathophysiology of depression with a Swiss army knife. *Neuron* 62, 453–455.
- Miyagi, S., Nishimoto, M., Saito, T., Ninomiya, M., Sawamoto, K., Okano, H., Muramatsu, M., Oguro, H., Iwama, A., and Okuda, A. (2006). The Sox2 regulatory region 2 functions as a neural stem cell-specific enhancer in the telencephalon. *J. Biol. Chem.* 281, 13374–13381.
- Moreno-Manzano, V., Rodríguez-Jiménez, F.J., Aceña-Bonilla, J.L., Fustero-Lardies, S., Erceg, S., Dopazo, J., Montaner, D., Stojkovic, M., and Sánchez-Puelles, J.M. (2010). FM19G11, a new hypoxia-inducible factor (HIF) modulator, affects stem cell differentiation status. *J. Biol. Chem.* 285, 1333–1342.
- Oppel, F., Müller, N., Schackert, G., Hendruschk, S., Martin, D., Geiger, K.D., and Temme, A. (2011). SOX2-RNAi attenuates S-phase entry and induces RhoA-dependent switch to protease-independent amoeboid migration in human glioma cells. *Mol. Cancer* 10, 137.
- Pastrana, E., Silva-Vargas, V., and Doetsch, F. (2011). Eyes wide open: a critical review of sphere-formation as an assay for stem cells. *Cell Stem Cell* 8, 486–498.
- Pevny, L.H., and Nicolis, S.K. (2010). Sox2 roles in neural stem cells. *Int. J. Biochem. Cell Biol.* 42, 421–424.
- Pilhatsch, M., Winter, C., Nordström, K., Vennström, B., Bauer, M., and Juckel, G. (2010). Increased depressive behaviour in mice harboring the mutant thyroid hormone receptor alpha 1. *Behav. Brain Res.* 214, 187–192.
- Pitt-Rivers, R. (1963). Biochemistry and physiology of thyroid hormones. *N. Y. State J. Med.* 63, 43–49.
- Samuels, M.H. (2008). Cognitive function in untreated hypothyroidism and hyperthyroidism. *Curr. Opin. Endocrinol. Diabetes Obes.* 15, 429–433.
- Sikorska, M., Sandhu, J.K., Deb-Rinker, P., Jezierski, A., Leblanc, J., Charlebois, C., Ribocco-Lutkiewicz, M., Bani-Yaghoob, M., and Walker, P.R. (2008). Epigenetic modifications of SOX2 enhancers, SRR1 and SRR2, correlate with in vitro neural differentiation. *J. Neurosci. Res.* 86, 1680–1693.
- Takanaga, H., Tsuchida-Straeten, N., Nishide, K., Watanabe, A., Aburatani, H., and Kondo, T. (2009). Gli2 is a novel regulator of sox2 expression in telencephalic neuroepithelial cells. *Stem Cells* 27, 165–174.
- Tavazoie, M., Van der Veken, L., Silva-Vargas, V., Louissaint, M., Colonna, L., Zaidi, B., Garcia-Verdugo, J.M., and Doetsch, F. (2008). A specialized vascular niche for adult neural stem cells. *Cell Stem Cell* 3, 279–288.
- Tomioka, M., Nishimoto, M., Miyagi, S., Katayanagi, T., Fukui, N., Niwa, H., Muramatsu, M., and Okuda, A. (2002). Identification of Sox-2 regulatory region which is under the control of Oct-3/4-Sox-2 complex. *Nucleic Acids Res.* 30, 3202–3213.
- Van Hooser, A., Goodrich, D.W., Allis, C.D., Brinkley, B.R., and Mancini, M.A. (1998). Histone H3 phosphorylation is required for the initiation, but not maintenance, of mammalian chromosome condensation. *J. Cell Sci.* 111, 3497–3506.
- Venero, C., Guadaño-Ferraz, A., Herrero, A.I., Nordström, K., Manzano, J., de Escobar, G.M., Bernal, J., and Vennström, B. (2005). Anxiety, memory impairment, and locomotor dysfunction caused by a mutant thyroid hormone receptor alpha1 can be ameliorated by T3 treatment. *Genes Dev.* 19, 2152–2163.
- Wiebe, M.S., Wilder, P.J., Kelly, D., and Rizzino, A. (2000). Isolation, characterization, and differential expression of the murine Sox-2 promoter. *Gene* 246, 383–393.
- Williams, G.R., and Bassett, J.H. (2011). Deiodinases: the balance of thyroid hormone: local control of thyroid hormone action: role of type 2 deiodinase. *J. Endocrinol.* 209, 261–272.
- Zhao, Z., Andersen, S.U., Ljung, K., Dolezal, K., Miotk, A., Schultheiss, S.J., and Lohmann, J.U. (2010). Hormonal control of the shoot stem-cell niche. *Nature* 465, 1089–1092.



MÉCANIQUE QUANTIQUE

Deux interprétations ?

L'interprétation actuelle de la mécanique quantique est née au congrès Solvay de 1927 où le point de vue de Niels Bohr, Werner Heisenberg, Max Born et Wolfgang Pauli s'est imposé contre celui de Max Planck, Albert Einstein, Louis de Broglie et Erwin Schrödinger : il fallait renoncer désormais au déterminisme et à l'existence d'une réalité objective. Les conséquences philosophiques et épistémologiques de cette interprétation sont immenses... et les difficultés de compréhension aussi !

PAR ALEXANDRE GONDRAN, ENSEIGNANT-CHERCHEUR À L'ÉCOLE NATIONALE D'AVIATION CIVILE, ET MICHEL GONDRAN, MEMBRE DE L'ACADÉMIE EUROPÉENNE INTERDISCIPLINAIRE DES SCIENCES

C'est en 1924 que Louis de Broglie (1892-1987) émet l'hypothèse que toute particule possède un caractère ondulatoire : c'est la dualité onde-corpuscule, une prédiction qui se révèle juste et dont la portée philosophique est considérable. Pour de Broglie, cette dualité s'exprime par le fait que toute particule est accompagnée d'une onde. Cependant, l'année suivante, Werner Heisenberg (1901-1976) met sur pied la mécanique dite matricielle. Dans cette théorie, il n'y a *a priori* ni onde, ni particule. Pour de Broglie et Albert Einstein (1879-1955), la physique était en train de s'engager dans une mauvaise voie : elle n'a plus comme ambition de décrire la réalité mais uniquement de prévoir des événements. La théorie de Heisenberg reçoit en revanche le soutien de Niels Bohr (1885-1962), Max Born (1882-1970), Wolfgang Pauli (1900-1958) et de la majorité des physiciens pour qui la particule ne se trouve nulle part tant qu'elle n'a pas été

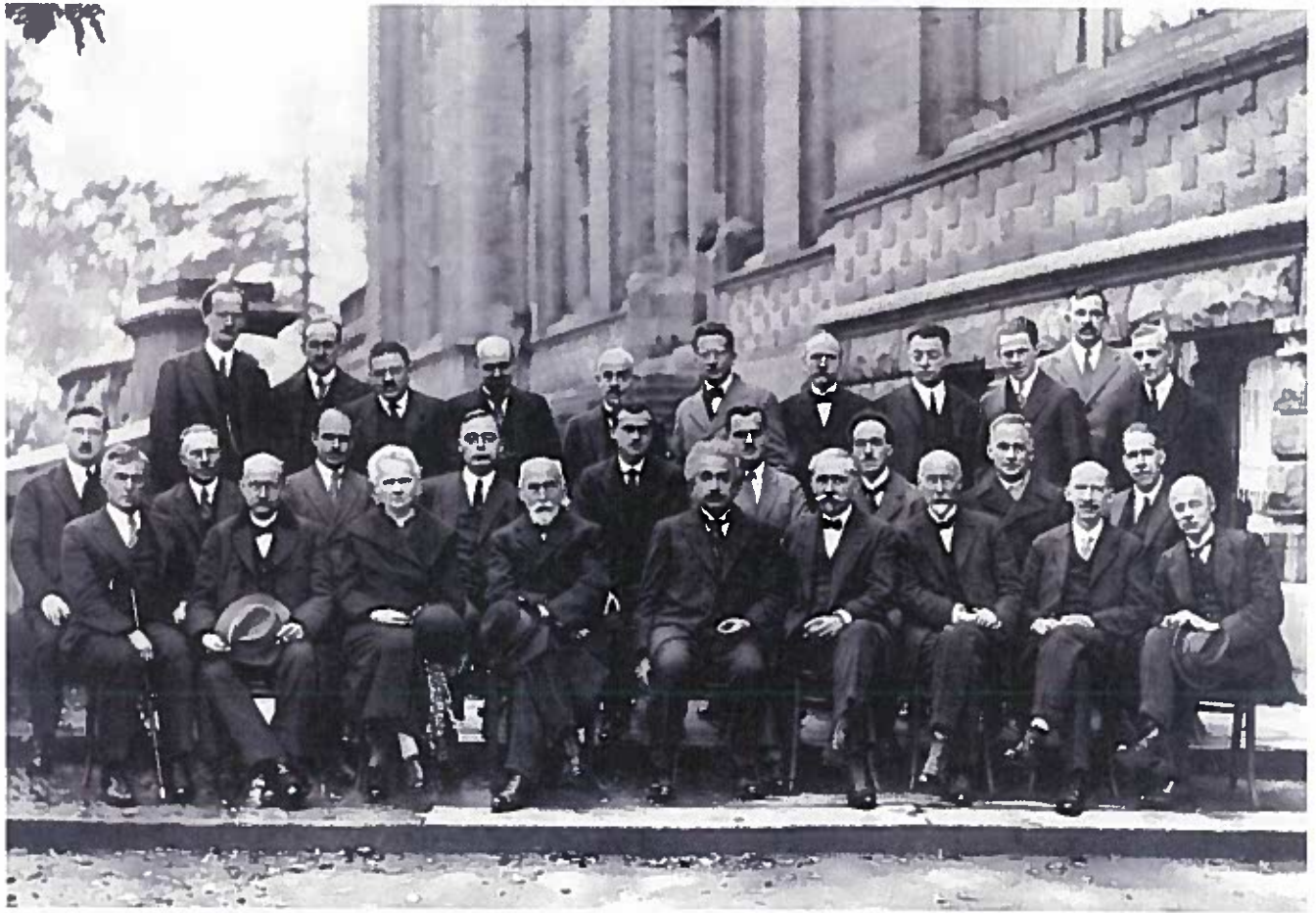
observée. De Broglie et Einstein sont persuadés quant à eux qu'elle existe indépendamment de son observation et se trouve donc à chaque instant quelque part. Cet article propose de remonter aux sources de ce débat, c'est-à-dire à l'interprétation de la fonction d'onde : cet objet mathématique abstrait qui permet de décrire les particules quantiques – photon, électron, atome, molécule... À travers l'expérience fondamentale des fentes de Young, nous présentons la théorie de l'onde pilote de de Broglie-Bohm (appelée *Bohmien Mechanics* dans le monde anglo-saxon) qui, en accord avec tous les résultats expérimentaux, réhabilite le réalisme* et le déterminisme*.

Les deux pères de la dualité onde-particule

FONCTION D'ONDE ET THÉORIE QUANTIQUE

À la fin du XIX^e siècle, la physique est construite sur deux concepts. D'un côté, il y a les particules, corpuscules de matière dont le mouvement est

* Les termes suivis d'un astérisque sont définis dans le glossaire situé en fin d'article.



Participants au congrès Solvay de 1927. Au premier rang, de gauche à droite : Irving Langmuir, Max Planck, Marie Curie, Hendrik Lorenz, Albert Einstein, Paul Langevin, Charles-Eugène Guye, Charles Thomson Rees Wilson, Owen Willans Richardson. Deuxième rang : Peter Debye, Martin Knudsen, William Lawrence Bragg, Hendrik Anthony Kramers, Paul Dirac, Arthur Compton, Louis de Broglie, Max Born, Niels Bohr. Troisième rang : Auguste Piccard, Émile Henriot, Paul Ehrenfest, Édouard Herzen, Théophile de Donder, Erwin Schrödinger, Jules-Émile Verschaffelt, Wolfgang Pauli, Werner Heisenberg, Ralph H. Fowler, Léon Brillouin. © B. Couprie pour le compte de l'Institut international de physique Solvay, parc Léopold, Bruxelles, Belgique.



décrit par la mécanique newtonienne. De l'autre, il y a les ondes, parmi lesquelles la lumière, qui possèdent des propriétés typiques : elles diffractent et interfèrent. C'est en 1900 que Max Planck (1858-1947), pour comprendre le rayonnement des corps chauffés, émit l'hypothèse que les échanges d'énergie entre matière et lumière ne s'effectuent pas de façon continue mais *via* des quantités discrètes (quanta d'énergie). En 1905, Einstein élabora cette notion de quanta d'énergie pour définir la lumière et introduisit ce qui fut appelé par la suite le photon : un grain insécable de lumière. Pendant les vingt années suivantes, le développement de la

théorie quantique fut riche non seulement d'hypothèses hardies et d'intuitions géniales, mais aussi d'âpres controverses. Après les modèles *ad hoc* de l'atome d'hydrogène de Bohr en 1913, c'est à de Broglie que revint le mérite « de lever un coin de la grand-voile » (selon les dires d'Einstein) en 1923, en émettant l'hypothèse qu'à toute particule de matière de masse m pouvait correspondre une onde de longueur d'onde $\lambda = h / mv$, v étant la vitesse et h la constante de Planck. La séparation onde-particule du XIX^e siècle vole définitivement en éclat. Le nouvel outil mathématique que de Broglie introduit pour décrire un objet quantique (électron, atome,

« Einstein, de Broglie et Schrödinger n'ont cessé d'insister sur ce que l'interprétation statistique de la mécanique quantique avait de peu satisfaisant, de réclamer un retour aux conceptions de la physique classique newtonienne et de proposer des moyens d'y arriver sans contredire aux faits expérimentaux. » (Discours de Max Born, colauréat du prix Nobel de physique, 1954.)

molécule...) porte le nom de *fonction d'onde*. Cependant, cette dernière reste une notion mathématique abstraite et sa signification réelle n'est pas définie clairement ; elle explique correctement le comportement ondulatoire des objets quantiques mais la notion classique de position n'est plus définie directement. En effet, à partir de cette fonction d'onde, Born montre en 1926 que seule la probabilité de la position de la particule peut être déterminée, sa position exacte demeurant inconnue. La théorie naissante ne prévoit que des probabilités ! C'est une révolution conceptuelle majeure.

Les équations de la théorie permettant de calculer l'évolution dans le temps de cette fonction d'onde (et donc des probabilités) furent inventées de manière indépendante par Heisenberg en 1925 et Erwin Schrödinger (1887-1961) en 1926, puis par Paul Dirac (1902-1984) en 1928 dans sa version plus complète où l'on tient compte de la relativité einsteinienne. Pauli, Pascual Jordan (1902-1980), puis Richard Feynman (1918-1988) et bien d'autres en feront la belle théorie conceptuelle connue aujourd'hui sous le nom de mécanique quantique.

Bien que la théorie quantique ne prévoie que des probabilités, elle va remporter un succès considérable. En effet, elle permet d'expliquer et d'anticiper les mesures effectuées sur le monde physique qui nous entoure avec une très grande précision, depuis la structure de l'atome jusqu'à la conduction électronique des solides. Cette théorie quantique constitue aujourd'hui un cadre essentiel à notre prévisibilité de la Nature, de l'infiniment petit à l'infiniment grand. De nombreuses applications en découlent : lasers, horloges atomiques, GPS (Global Positioning System, le géo-positionnement par satellite), ordinateurs, IRM (imagerie par résonance magnétique)...

L'EXPÉRIENCE DES FENTES DE YOUNG

Mais c'est l'interprétation de la fonction d'onde de la mécanique quantique qui déclenche le plus grand débat scientifique du XX^e siècle. La fonction d'onde représente-t-elle *complètement* l'objet quantique comme l'assure l'interprétation statistique de Copenhague (p. 33) ? Dans ce cas, les probabilités sont fondamentales à la nature

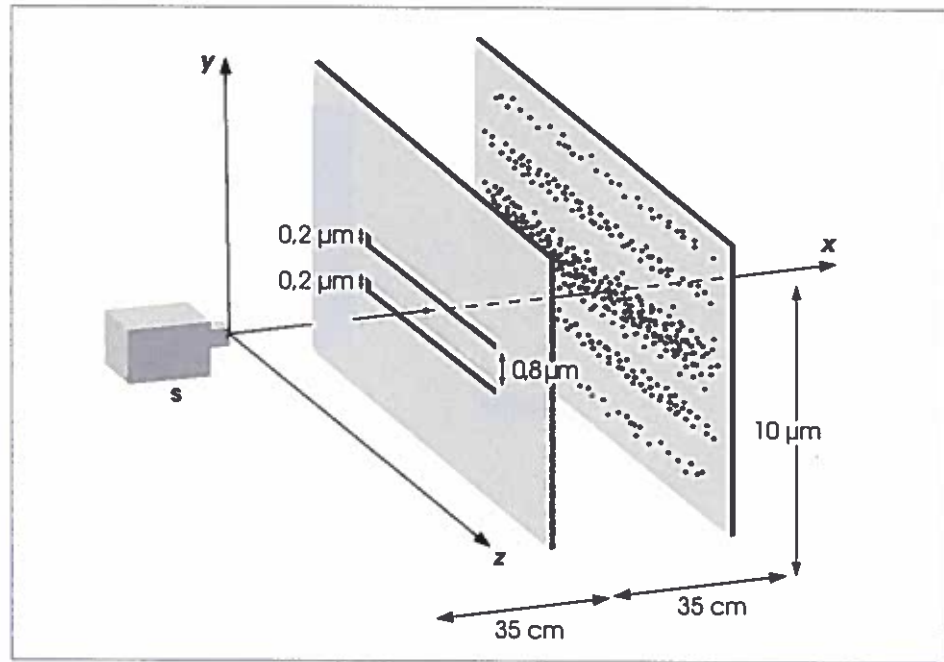


Figure 1. Schéma de l'expérience de Young réalisée par Claus Jönsson avec des électrons. © A. Gondran.

physique. Ou alors faut-il ajouter à la fonction d'onde la position de la particule pour représenter l'objet quantique, comme le veut l'interprétation déterministe de de Broglie-Bohm ? Dans ce cas, les probabilités proviennent d'un modèle sous-jacent de la réalité.

L'expérience des fentes de Young a été réalisée initialement par Thomas Young (1773-1829) en 1804 et a démontré l'aspect ondulatoire de la lumière ; plus de cent ans plus tard, elle s'avère cruciale dans le débat sur l'interprétation du dualisme onde-particule. En effet, c'est une expérience simple qui présente les deux caractéristiques des phénomènes quantiques : les caractères ondulatoire au niveau macroscopique et corpusculaire au niveau microscopique.

« [Cette expérience aborde] le point fondamental du comportement mystérieux [des objets quantiques (photon, électron, atome, molécule...)] sous son aspect le plus étrange. C'est un phénomène qu'il est

impossible, absolument impossible à expliquer de façon classique et qui contient le cœur de la mécanique quantique. En réalité, il en contient l'unique mystère. » (Richard Feynman.)

La figure 1 présente le schéma de l'expérience des fentes de Young réalisée par Claus Jönsson. Un canon émet des électrons dans le plan horizontal, à travers un trou de quelques millimètres. Ces derniers rencontrent une plaque percée de deux fentes horizontales. Un écran situé après ces fentes récolte les électrons un à un (aspect corpusculaire). L'impact de chaque électron apparaît sur l'écran au fur et à mesure que l'expérience se déroule. Au bout de quelques milliers d'impacts d'électrons, leur répartition sur l'écran fait apparaître des franges d'interférence (alternance de zones où les impacts sont nombreux et de zones où il n'y en a aucun, caractéristique de l'aspect ondulatoire). Le caractère ondulatoire d'un électron ne se révèle que statistiquement.

Interprétation de Copenhague

Dans l'interprétation de Copenhague, qui est l'interprétation orthodoxe de la mécanique quantique, toujours en vigueur, l'électron est soit *une onde* soit *un corpuscule*, mais en aucun cas les deux à la fois. C'est le *principe de complémentarité de Bohr* pour lequel l'électron présente soit les propriétés d'une onde, soit celles d'un corpuscule. Durant toute l'expérience, l'électron est seulement une onde qui traverse les deux fentes à la fois (fig. 2) ; il ne manifeste sa propriété corpusculaire qu'au moment de l'impact sur l'écran, phénomène appelé *postulat de réduction du paquet d'onde*. L'équation de Schrödinger ne prévoit qu'une probabilité du lieu de l'impact, égale au carré de l'amplitude de l'onde. Sa position effective dans l'interprétation de Copenhague est sans explication : c'est un aléa fondamental. Einstein critiqua cette vision des choses par sa célèbre formule : « Dieu ne joue pas aux dés ». D'après lui, les prédictions aléatoires de la mécanique quantique ne provenaient pas d'un aléa « vrai » ou fondamental de la physique, mais d'une incomplétude du modèle : il devait exister un modèle sous-jacent qui explique ces aléas.

Un autre problème déroutant de cette interprétation est qu'elle présente deux possibilités d'évolution de la fonction d'onde : soit grâce à l'équation de Schrödinger (dans la plupart des cas), soit grâce à la réduction du paquet d'onde (dès qu'une mesure est effectuée), la théorie ne préconisant rien sur le choix à faire. Qu'est-ce qui différencie une interaction « normale » (équation de Schrödinger) d'une interaction relevant de la mesure (réduction du paquet d'onde) ? La théorie de la décohérence* ne règle en aucun cas ce problème. Elle s'intéresse seulement à l'enchaînement des interactions successives avec l'appareil de mesure, ce qui

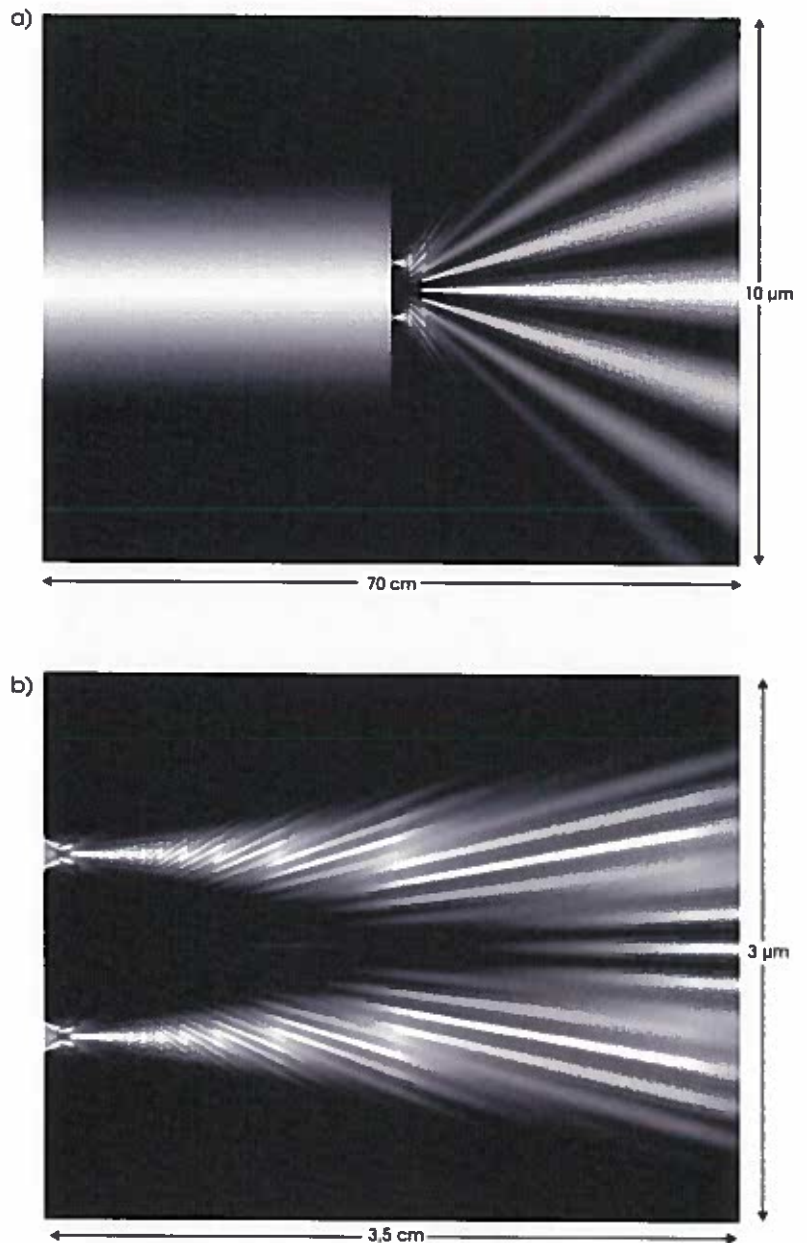


Figure 2. a) Densité de probabilité de présence d'un électron à différentes distances des fentes. Elle est commune aux interprétations de Copenhague et de de Broglie-Bohm. b) Zoom sur la densité de la figure 2a : probabilité de présence d'un électron à différentes distances des fentes. Elle est commune aux deux interprétations. © A. Gondran.

« En 1952, j'ai vu l'impossible se réaliser. David Bohm montrait explicitement comment des paramètres pouvaient effectivement être introduits, dans la mécanique ondulatoire non relativiste, grâce auxquels la description indéterministe pouvait être transformée en une description déterministe. » (John Bell.)



aboutit à l'intrication* d'une particule quantique individuelle avec un élément macroscopique. Cette intrication correspond à la célèbre critique de Schrödinger connue sous le nom de chat de Schrödinger (encadré). Une critique approfondie de cette non-consistance de l'interprétation de Copenhague peut se trouver dans les excellents livres de Franck Laloë et Jean Bricmont (*Pour en savoir plus*). Ces problèmes expliquent largement la difficulté de compréhension de la mécanique quantique. L'interprétation de Copenhague nie même l'existence de la réalité avant la mesure par un observateur. Einstein cristallise sa critique par la formule : « j'aime à penser que la Lune est là, même quand je ne la regarde pas ».

Interprétation de de Broglie-Bohm

UNE THÉORIE SOLIDE...

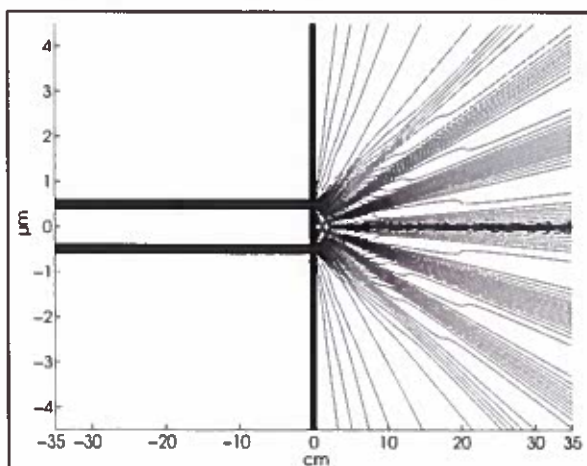
Dans l'interprétation de de Broglie-Bohm, l'électron est à la fois *une onde* et *un corpuscule*. Onde et corpuscule coexistent, la première guidant le second, d'où le nom d'*onde pilote* donné par de Broglie en 1927. L'électron est donc décrit par la fonction d'onde et par la position de son centre de gravité. Il correspond à une *réalité augmentée* par rapport à la mécanique classique : il n'y

a pas d'aléa fondamental, c'est la position initiale de l'électron (au sortir du canon) qui détermine son impact sur l'écran et, dans ce cas, « Dieu ne joue pas aux dés ». Comme dans le chaos déterministe, de petites variations dans les conditions initiales (positions différentes des électrons au sortir du canon) engendrent de grandes variations au final (impacts sur l'écran) (fig. 3). Cependant, du fait que la position initiale de l'électron n'est connue que statistiquement, la position finale ne peut, elle aussi, être connue en pratique que statistiquement. Comme l'a formulé Bernard d'Espagnat (*Pour en savoir plus*), la « réalité est voilée », c'est-à-dire qu'elle ne nous est pas directement accessible : à la sortie du canon à électrons, il nous est impossible de connaître la position exacte de chaque électron.

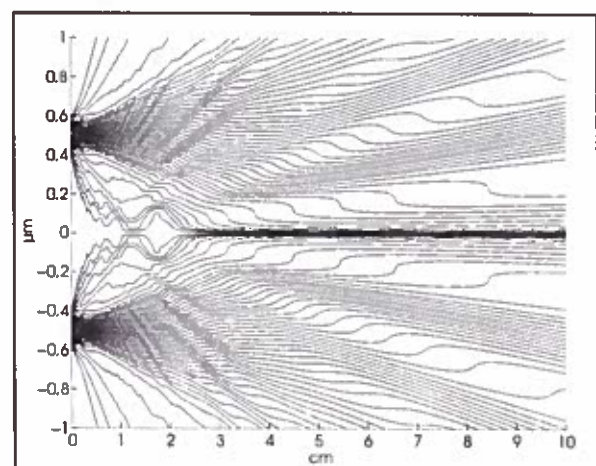
Dans cette théorie de de Broglie-Bohm, la notion de trajectoire pour le centre de gravité de l'électron est rétablie, sa vitesse se déduisant directement de sa fonction d'onde. Contrairement à l'interprétation de Copenhague, il n'y a pas de frontière entre les mondes classique et quantique, le passage de l'un à l'autre se fait continûment. Comme le montre la figure 4, les trajectoires quantiques convergent vers les trajectoires classiques lorsque, dans les simulations, on fait tendre la constante de Planck h vers 0.

Chat de Schrödinger

Il s'agit d'une expérience de pensée proposée par Erwin Schrödinger en 1935 pour mettre en lumière le problème d'inconsistance de la mesure dans l'interprétation de Copenhague. Un chat est enfermé dans une boîte contenant un dispositif qui le tue dès qu'un atome radioactif se désintègre (en cassant une fiole qui libère un poison mortel). Avant de se désintégrer, l'atome est dans une superposition des états désintégré et intact. Selon l'interprétation de Copenhague, l'atome se trouve simultanément dans deux états ; cette interprétation de la superposition d'états ne considère pas l'état de l'atome comme un véritable état intermédiaire (comme le violet est entre le rouge et le bleu) mais comme un état indéterminé. Le problème survient car dans le monde classique (macroscopique), ces états indéterminés n'existent pas ou du moins n'ont jamais été observés. Les lois de la mécanique quantique (équation de Schrödinger) prévoient pourtant que la superposition d'états de l'atome se propage de proche en proche aux autres objets quantiques, qui se trouvent à leur tour dans une superposition d'états. Ces superpositions se propagent alors à des objets de plus en plus gros, jusqu'à la fiole contenant le poison, à la fois dans les états « cassé » et « intact », et finalement au chat à la fois mort et vivant. Il est possible de sortir de ce dilemme de deux manières. La première en ajoutant un postulat supplémentaire à la mécanique quantique, celui de la réduction du paquet d'onde énoncé dans l'interprétation de Copenhague. Cette nouvelle loi d'évolution du système quantique suppose que lorsqu'une « mesure » est effectuée par un « observateur », l'indétermination du système se lève : le système se met spontanément et instantanément dans l'un des deux états de façon aléatoire (aléa fondamental). Dans le cas du chat, c'est l'ouverture de la boîte qui le contraint à se mettre soit dans l'état « mort » soit dans l'état « vivant ». Reste une question non résolue : quand utiliser le postulat de réduction du paquet d'onde ? Et l'équation de Schrödinger ? En effet, ce sont deux façons différentes de faire évoluer le système. En d'autres termes, qu'est-ce qui différencie une « mesure » d'une interaction classique ? L'autre possibilité pour sortir du dilemme est de remettre en question l'interprétation de la superposition d'états : ce que fait l'interprétation de de Broglie-Bohm en complétant la description du système quantique. L'état de superposition est un état réel, intermédiaire entre les deux états et il existe une variable supplémentaire (la position de la particule) qui lève l'indétermination. Comme dans le jeu de pile ou face, la pièce de monnaie qui virevolte dans l'air est dans une superposition de l'état pile et de l'état face avant d'être mesurée, mais seuls les états pile et face sont observables.



a)



b)

Figure 3. a) Simulation de trajectoires possibles pour l'expérience des fentes de Young. Les positions initiales des électrons à la sortie du canon sont tirées aléatoirement. b) Zoom des trajectoires. © A. Gondran.

Alexandre Gondran

Après des études d'ingénieur (Télécom Paris, 2001) et un doctorat en informatique (université technologique de Belfort-Montbéliard, 2008), Alexandre Gondran est actuellement enseignant-chercheur à l'École nationale d'aviation civile à Toulouse. Il a travaillé également au département de physique du Palais de la découverte et enseigné en secondaire la physique-chimie.

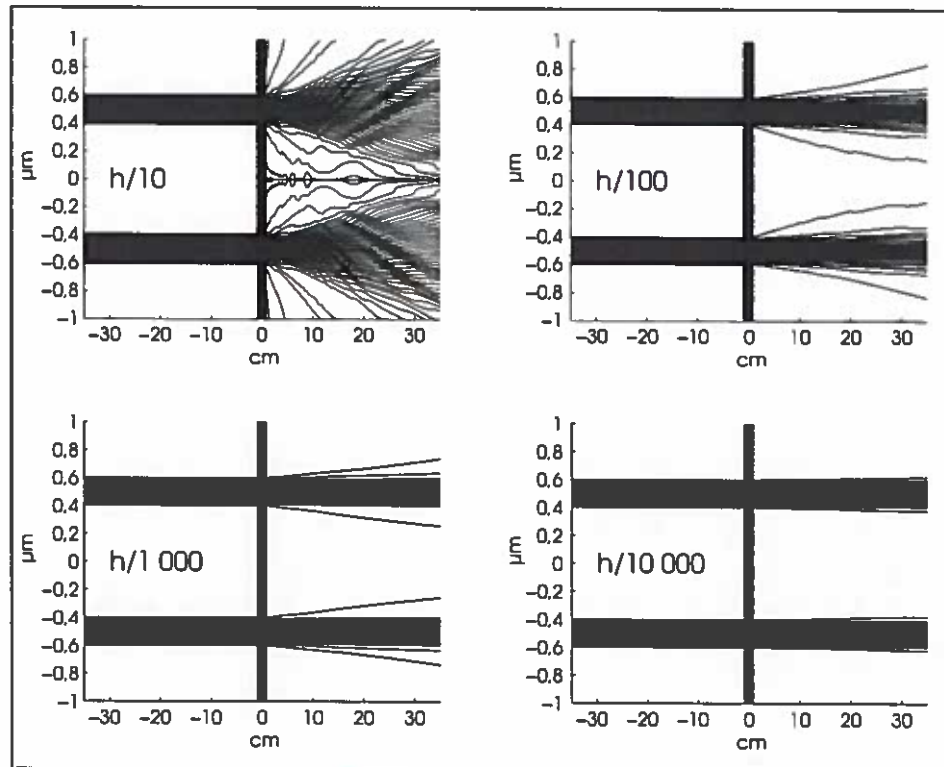


Figure 4. Convergence des trajectoires quantiques vers les trajectoires classiques lorsque, dans les simulations, on fait tendre la constante de Planck h vers 0. © A. Gondran.

En outre, cette théorie prédit les mêmes résultats que la mécanique quantique habituelle dont elle partage les équations. Elle complète le modèle et rétablit déterminisme et réalisme en mécanique quantique. Aucune expérience actuelle n'est venue invalider cette théorie ; au contraire, toutes les expériences l'ont confirmée, en particulier celles de non-localité d'Aspect (expérience EPR, Einstein-Podolsky-Rosen) et la cryptographie quantique. Les expériences réalisées en 1981 et 1982 par l'équipe d'Alain Aspect ont montré de façon certaine que si deux particules ayant interagi ensemble d'une certaine manière (on dit qu'elles sont intriquées), alors il n'est plus possible d'expliquer le comportement de l'une sans connaître celui de l'autre. Et même si les particules sont très éloignées, l'interaction de l'une sur l'autre est instantanée (ou du moins supralimi-

naire) et ne décroît pas avec la distance. On parle de façon équivalente soit de non-localité, c'est-à-dire que les deux particules forment un tout même si elles sont très éloignées l'une de l'autre, soit d'interaction à distance instantanée. À noter que cette interaction a été observée uniquement sur les spins des particules et non sur leurs positions ou leurs vitesses. Ce comportement surprenant de la physique quantique a été signalé dès 1935 dans une expérience de pensée imaginée par Einstein, Boris Podolsky (1896-1966) et Nathan Rosen (1909-1995) – c'est pourquoi on parle d'expérience EPR. Bien que la théorie de de Broglie-Bohm ait été développée en 1927, elle prévoit cette interaction non locale.

La cryptographie quantique est une application récente de la mécanique quantique (1984), qui permet de transmettre des messages en étant certain que personne n'a écouté le message

entre son émission et sa réception. Elle utilise la superposition d'états du spin d'un photon et le fait que le spin est une propriété à valeur non préexistante, c'est-à-dire que toute mesure du spin transforme la valeur qu'elle avait avant la mesure. Certaines versions de la cryptographie quantique utilisent également l'intrication quantique.

... MAIS DÉLAISSÉE

Pourtant, cette interprétation reste méconnue des physiciens et ignorée du grand public. En 1987, John Bell (1928-1990) évoque son incompréhension quant aux difficultés de cette théorie à être reconnue : « Mais alors pourquoi Born ne m'avait-il pas parlé de cette « onde pilote » ? Ne serait-ce que pour signaler ce qui n'allait pas avec elle ? Pourquoi Von Neumann ne l'a-t-il pas envisagée ? Plus extraordinaire encore, pourquoi des gens ont-ils continué à produire des preuves d'impossibilité, après 1952, et aussi récemment qu'en 1978 ? Alors que même Pauli, Rosenfeld et Heisenberg ne pouvaient guère produire de critique plus dévastatrice de la théorie de Bohm que de la dénoncer comme étant « métaphysique » et « idéologique » ? Pourquoi

l'image de l'onde pilote est-elle ignorée dans les cours ? Ne devrait-elle pas être enseignée, non pas comme l'unique solution, mais comme un antidote à l'autosatisfaction dominante ? Pour montrer que le flou, la subjectivité et l'indéterminisme ne nous sont pas imposés de force par les faits expérimentaux, mais proviennent d'un choix théorique délibéré ? » A. G. et M. G.

Pour en savoir plus

> thequantumphysics.wordpress.com

Bricmont J., « Contre la philosophie de la mécanique quantique », in Franck R. (éd.), *Les sciences et la philosophie – Quatorze essais de rapprochement*, Vrin, 1995.

Bricmont J., Zwirn H., *Philosophie de la mécanique quantique*, Vuibert, 2009.

D'Espagnat B., *Le réel voilé – Analyse des concepts quantiques*, Fayard, 1994 ; *Une incertaine réalité – Le monde quantique, la connaissance et la durée*, Fayard, 1993 ; *À la recherche du réel – Le regard d'un physicien*, Pocket, 1991.

Gondran M., Gondran A., *Mécanique quantique : et si Einstein et de Broglie avaient aussi raison ?*, Éditions Matériologiques, 2014.

Lalô F., *Comprenons-nous vraiment la mécanique quantique ?*, EDP Sciences, 2011. Lire aussi : <http://www.phys.ens.fr/cours/notes-de-cours/fmq/mq.PDF>.

Michel Gondran

Michel Gondran a fait toute sa carrière à EDF R&D en tant qu'ingénieur-chercheur et conseiller scientifique.

Ses recherches pluridisciplinaires l'ont amené à enseigner dans de nombreuses écoles et à l'université (École polytechnique, ENSAE, Ponts et Chaussées, ENSTA, université Paris-Dauphine). Il est membre de l'Académie européenne Interdisciplinaire des sciences (président 2005-2010). Il est lauréat de l'Académie des sciences et de l'Académie des inscriptions et belles-lettres.

Glossaire

Décohérence : phénomène étudié initialement par David Bohm (1917-1992) en 1952 qui s'intéresse à l'enchaînement des interactions d'un objet quantique avec les objets quantiques de son environnement. Ces interactions successives intriquent les objets quantiques de l'environnement avec l'objet quantique initial et rendent le système global très instable car une « mesure » de l'un des objets de l'environnement a des effets sur tous les autres objets quantiques dont l'objet initial. Si ce dernier est dans un état superposé, tous les objets de l'environnement deviennent

à leur tour des états superposés ; c'est le cas du chat de Schrödinger. La décohérence est la perte de cette superposition.

Déterminisme : un événement est déterministe s'il s'explique grâce à d'autres événements par une suite de causes et d'effets ; il n'existe pas d'événement fondamentalement aléatoire, c'est-à-dire sans cause. L'aléa s'explique par l'ignorance des conditions initiales de l'expérience ou de l'incomplétude du modèle s'il est trop complexe ; par exemple la météo, le billard, le loto ou le lancer de dés.

Intrication : après que deux particules ont interagé ensemble, il se peut qu'il ne soit plus possible d'expliquer le comportement de l'une sans connaître le comportement de l'autre. Elles forment un tout, on dit qu'elles sont intriquées.

Réalisme : il consiste à admettre qu'il existe une réalité objective, c'est-à-dire indépendante de l'observateur. Il est nécessaire de préciser la nature de ce réel sous-jacent à notre perception.

Replacing the Singlet Spinor of the EPR-B Experiment in the Configuration Space with Two Single-Particle Spinors in Physical Space

Michel Gondran¹ · Alexandre Gondran²

Received: 21 April 2015 / Accepted: 7 April 2016
© Springer Science+Business Media New York 2016

Abstract Recently, for spinless non-relativistic particles, Norsen (Found Phys 40:1858–1884, 2010) and Norsen et al. (Synthese 192:3125–3151, 2015) show that in the de Broglie–Bohm interpretation it is possible to replace the wave function in the configuration space by single-particle wave functions in physical space. In this paper, we show that this replacement of the wave function in the configuration space by single-particle functions in the 3D-space is also possible for particles with spin, in particular for the particles of the EPR-B experiment, the Bohm version of the Einstein–Podolsky–Rosen experiment.

Keywords EPR · Bohm · Nonlocality · Bell · Configuration space

1 Introduction

A major difficulty of the wave function interpretation of N particles in quantum mechanics is its definition in a $3N$ -dimensional configuration space. Since the Solvay Conference in 1927, de Broglie and Schrödinger considered the wave function of N particles introduced by Schrödinger in the $3N$ -dimensional configuration space as fictitious and proposed to replace it by N single-particle wave functions in 3D-space:

✉ Michel Gondran
michel.gondran@polytechnique.org

Alexandre Gondran
alexandre.gondran@enac.fr

¹ University Paris Dauphine, Lamsade, 75016 Paris, France

² Ecole Nationale de l'Aviation Civile, 31000 Toulouse, France

It appears to us certain that if one wants to *physically* represent the evolution of a system of N corpuscles, one must consider the propagation of N waves in space, each N propagation being determined by the action of the N-1 corpuscles connected to the other waves. Nevertheless, if one focusses one's attention only on the corpuscles, one can represent their states by a point in configuration space, and one can try to relate the motion of this representative point to the propagation of a fictitious wave Ψ in configuration space. It appears to us very probable that the wave

$$\Psi = a(q_1, q_2, \dots, q_n) \cos \frac{2\pi}{h} \varphi(t, q_1, \dots, q_n),$$

a solution of the Schrödinger equation, is only a fictitious wave, which in the *Newtonian approximation*, plays for the representative point of the system in configuration space the same role of pilot wave and of probability wave that the wave Ψ plays in ordinary space in the case of a single material point. (Louis de Broglie [3], cited by Norsen [1])

This use of the q-space [configuration space] is to be seen only as a mathematical tool, as it is often applied also in the old mechanics; ultimately... the process to be described is one in space and time. (Erwin Schrödinger [4], cited by Norsen et al. [2] p. 26)

However, this program to replace the wave function in a 3N-dimensional configuration space by N single-particle wave functions was prematurely abandoned. It was recently re-opened by Norsen et al. [1,2]. For spinless non-relativistic particles, these authors show that it is possible in the de Broglie-Bohm pilot-wave theory to replace the wave function in the configuration space by N single-particle wave functions in physical space [2]. These N wave functions in 3D space are the N *conditional wave functions* of a subsystem introduced by Dürr et al. [6,7]. For a N-particle wave function $\Psi(x_1, x_2, \dots, x_N, t)$, the N conditional wave functions are:

$$\Psi_1(x, t) = \Psi(x, x_2, \dots, x_N, t)|_{x_2=X_2(t);x_N=X_N(t)}$$

$$\Psi_2(x, t) = \Psi(x_1, x, \dots, x_N, t)|_{x_1=X_1(t);x_N=X_N(t)}$$

$$\Psi_N(x, t) = \Psi(x_1, \dots, x_{N-1}, x, t)|_{x_1=X_1(t);x_{N-1}=X_{N-1}(t)}$$

where $X_i(t)$ is the position of the particle i at time t in the Bohmian mechanics. The evolutions of these positions $X(t) = \{X_1(t), X_2(t), \dots, X_N(t)\}$ are given by the guidance formula:

$$\frac{dX_i(t)}{dt} = \frac{\hbar}{m_i} \text{Im} \frac{\nabla_i \Psi}{\Psi} |_{\mathbf{x}=\mathbf{X}(t)} \equiv \frac{\hbar}{m_i} \text{Im} \frac{\nabla \Psi_i}{\Psi_i} |_{x=X_i(t)}$$

The aim of this paper is to show that this replacement of the wave function in the configuration space by single-particle functions in the 3D space is also possible in the de Broglie-Bohm interpretation for particles with spin, in particular for the particles in the singlet state of the EPR-B experiment, the Bohm version of the Einstein-Podolsky-Rosen experiment.

To realize, in Bohmian mechanics, this decomposition, we use an explicit solution of the wave function of the EPR-B experiment. The first analytic expression of the wave function and of the probability density for the EPR-B experiment was done in 1987 by Dewdney et al. [10] via a complete integration of the two-body Pauli equation *over time and space*. They give also the first causal interpretation of the EPR-B experiment [10, 11]. However, this interpretation presents a flaw: the spin module of each particle varied during the experiment from 0 to $\frac{\hbar}{2}$. The contribution of this paper is, first, to correct this flaw by considering a spin module always equal to $\frac{\hbar}{2}$, and, second, to replace the singlet spinor of two entangled particles by two single-particle spinors.

The rest of the paper is organized as follows: Sect. 2 recalls how Bohmian mechanics defines the spin of a quantum particle and how it interprets its measurement in a Stern–Gerlach apparatus. The explicit solution of the two-body Pauli equation *over time and space* for EPR-B experiment, is presented in Sect. 3. A new causal interpretation of the EPR-B experiment is proposed in Sect. 4, correcting the flaw of the previous studies and allowing to replace the singlet spinor by two single-particle spinors.

2 Spin and Its Measurement in Bohmian mechanics

In the Copenhagen interpretation, the state of a spin 1/2 particle is given by the wave function $\Psi(\mathbf{x}, t)$, called Pauli spinor, which has two complex components $\Psi^+(\mathbf{x}, t)$ and $\Psi^-(\mathbf{x}, t)$. The non-relativist evolution of the spinor $\Psi(\mathbf{x}, t) = \begin{pmatrix} \Psi^+(\mathbf{x}, t) \\ \Psi^-(\mathbf{x}, t) \end{pmatrix}$, for a neutral spin-1/2 particle with a mass m and a magnetic moment μ in a magnetic field \mathbf{B} , is given by the Pauli equation:

$$i\hbar \begin{pmatrix} \frac{\partial \Psi^+(\mathbf{x}, t)}{\partial t} \\ \frac{\partial \Psi^-(\mathbf{x}, t)}{\partial t} \end{pmatrix} = -\frac{\hbar^2}{2m} (\nabla)^2 \begin{pmatrix} \Psi^+(\mathbf{x}, t) \\ \Psi^-(\mathbf{x}, t) \end{pmatrix} + \mu \mathbf{B} \boldsymbol{\sigma} \begin{pmatrix} \Psi^+(\mathbf{x}, t) \\ \Psi^-(\mathbf{x}, t) \end{pmatrix} \tag{1}$$

where $\boldsymbol{\sigma} = (\sigma_1, \sigma_2, \sigma_3)$ corresponds to the three Pauli matrices.

In the de Broglie–Bohm interpretation, the wave function does not completely represent the state of the quantum particle and it is necessary to add the particle position $X(t)$. The evolution of the spinor is still given by the Pauli equation (1) and the evolution of the position is given by the guidance formula introduced by Takabayasi [8], Bohm et al. [9]:

$$\frac{dX(t)}{dt} = \frac{\hbar}{2m\rho} \text{Im}(\Psi^\dagger \nabla \Psi) \tag{2}$$

where $\Psi^\dagger = (\Psi^{+*}, \Psi^{-*})$ and $\rho = \Psi^\dagger \Psi$. A two-component spinor can be linked to the three Euler angles (θ, φ, χ) and we can write (cf. Bohm and Hiley [13], p. 206):

$$\Psi(\mathbf{x}, t) = \begin{pmatrix} \Psi^+(\mathbf{x}, t) \\ \Psi^-(\mathbf{x}, t) \end{pmatrix} = \sqrt{\rho} e^{i\chi} \begin{pmatrix} \cos \frac{\theta}{2} e^{i\frac{\varphi}{2}} \\ i \sin \frac{\theta}{2} e^{-i\frac{\varphi}{2}} \end{pmatrix},$$

where ρ, χ, θ and φ are functions of \mathbf{x} and t . Bohm et al. [9] define the spin vector as

$$\mathbf{s}(\mathbf{x}, t) = \frac{\hbar}{2\rho} \Psi^\dagger(\mathbf{x}, t) \boldsymbol{\sigma} \Psi(\mathbf{x}, t) = \frac{\hbar}{2} (\sin\theta \sin\varphi, \sin\theta \cos\varphi, \cos\theta). \tag{3}$$

More properly, $\mathbf{s}(\mathbf{x}, t)$ is a spin vector field: in each point of the 3D space, a vector is defined by the orientation of θ and φ . The spin vector of an individual particle defined by $\Psi(\mathbf{x}, 0)$ and $X(0)$ is given by the Eq. (3) evaluated along its trajectory $X(t)$:

$$\mathbf{s}(t) = \mathbf{s}(\mathbf{x}, t)|_{\mathbf{x}=X(t)} = \mathbf{s}(X(t), t). \tag{4}$$

The spin vector therefore depends on the spinor and on the position of the particle. As Dürr et al. remark [7]: *Unlike position, spin is not primitive, i.e., no actual discrete degrees of freedom, analogous to the actual positions of the particles, are added to the state description in order to deal with “particles with spin”. Roughly speaking, spin is merely in the wave function.*

In the de Broglie–Bohm interpretation, the initial wave function of a quantum particle, prepared with a spin vector having (θ_0, φ_0) as Euler angles, is described by a spinor as the following:

$$\Psi_0(x, z) = (2\pi\sigma_0^2)^{-\frac{1}{2}} e^{-\frac{x^2+z^2}{4\sigma_0^2}} \begin{pmatrix} \cos \frac{\theta_0}{2} e^{i\frac{\varphi_0}{2}} \\ \sin \frac{\theta_0}{2} e^{-i\frac{\varphi_0}{2}} \end{pmatrix} \tag{5}$$

$$= (2\pi\sigma_0^2)^{-\frac{1}{2}} e^{-\frac{x^2+z^2}{4\sigma_0^2}} \left(\cos \frac{\theta_0}{2} e^{i\frac{\varphi_0}{2}} |+\rangle + \sin \frac{\theta_0}{2} e^{-i\frac{\varphi_0}{2}} |-\rangle \right) \tag{6}$$

corresponding to a pure state.

Quantum mechanics textbooks [14–17] do not take into account the spatial extension of the spinor (5) and simply use the simplified spinor without spatial extension:

$$\Psi_0 = \begin{pmatrix} \cos \frac{\theta_0}{2} e^{i\frac{\varphi_0}{2}} \\ \sin \frac{\theta_0}{2} e^{-i\frac{\varphi_0}{2}} \end{pmatrix}. \tag{7}$$

This spatial extension enables, in following the precursory works of Takabayasi [8], Bohm et al. [9] and Dewdney et al. [10], to taking into account the spin evolution during the measurement. Indeed, the difference in the evolution of the spatial extension between the two spinor components has a key role in the explanation of the measurement process with Bohmian mechanics (cf. Eq. (32) in Appendix).

In the Stern–Gerlach experiment, the spin of equations (5) or (7) is not directly measured; its measurement is obtained, after passing through an electromagnet during a time Δt , from the impact of the particle on a screen located 20 cm after the Stern–Gerlach electromagnet. This distance corresponds to the time required to separate the initial wave packet into two disjoint packets; this is the *decoherence time* t_D (cf. Eq. (35) in Appendix).

The measurement of spin (up or down along the z-axis) has no a pre-existing value before measurement. For the spinor (5), the initial spin vector $\mathbf{s}(X(0), 0) =$

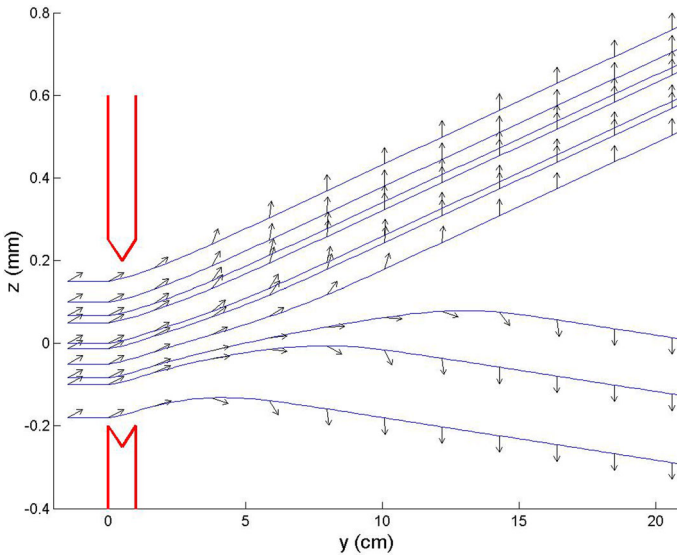


Fig. 1 Ten silver atom trajectories with the same initial spinor orientation ($\theta_0 = \frac{\pi}{3}$) and with 10 different initial positions z_0 ; arrows represent the spin orientation $\theta(z(t), t)$ along the trajectories

$\frac{\hbar}{2}(\sin \theta_0 \sin \varphi_0, \sin \theta_0 \cos \varphi_0, \cos \theta_0)$ does not depend on the initial position $X(0) = (x_0, y_0, z_0)$, but will evolve as $\mathbf{s}(X(t), t)$ differently during measurement depending on the initial position z_0 of the particle.

Figure 1 presents in the (Oyz) plane, 10 trajectories of silver atoms having the same initial spinor orientations ($\theta_0 = \frac{\pi}{3}, \varphi_0 = 0$) but having 10 different initial positions z_0 . Those initial positions z_0 have been randomly chosen from a Gaussian distribution with standard deviation σ_0 . The spin orientation $\theta(z(t), t)$ of each atom is represented by arrows.

The final orientation, obtained after the decoherence time t_D (Eq. (35) in Appendix), depends on the specific initial particle position z_0 in the spinor with a spatial extension and on the initial angle θ_0 of the spin with the z -axis. In previous works [11, 18], $\theta(t_D) = +\frac{\pi}{2}$ is obtained if $z_0 > z^{\theta_0}$ and $\theta(t_D) = -\frac{\pi}{2}$ if $z_0 < z^{\theta_0}$ with

$$z^{\theta_0} = \sigma_0 \Phi^{-1} \left(\sin^2 \frac{\theta_0}{2} \right) \tag{8}$$

where Φ is the cumulative distribution of the standard normal distribution. If we ignore the position of the atom in its wave function, we lose the determinism given by Eq. (8).

In the de Broglie–Bohm interpretation, the “measured” value is not a preexisting value. It is contextual and conforms to the Kochen and Specker theorem [12].

Finally, the Bohmian mechanics proposes a clear interpretation of the spin measurement in quantum mechanics. There is interaction with the measuring apparatus as Bohr said; and there is indeed a minimum time required to measure. However this measurement and this time do not have the meaning that is usually attributed to them. The result of the Stern–Gerlach experiment is not the measure of the spin projection along the z -axis, but the continuous orientation of the spin either in the direction of

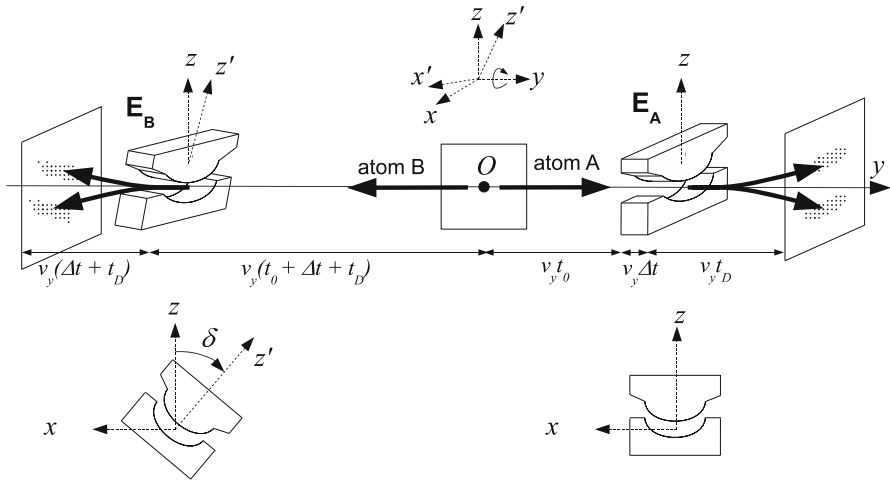


Fig. 2 Schematic configuration of the EPR-B experiment

the magnetic field gradient, or in the opposite direction. It depends on the position of the particle in the wave function. We have therefore a simple explanation for the non-compatibility of spin measurements along different axes. The measurement duration ($t \geq t_D$) is then the time necessary for the particle to point its spin in the final direction.

3 Explicit Solution of the Spinor in Configuration Space for the EPR-B Experiment

Figure 2 presents the Einstein–Podolsky–Rosen–Bohm experiment. A source S creates in O an entangled pair of identical atoms A and B, with opposite spins. The atoms A and B split following the y -axis in opposite directions (B with velocity v_0 , A with velocity $-v_0$), and head towards two identical Stern–Gerlach apparatuses \mathcal{A} and \mathcal{B} .

The electromagnet \mathcal{A} “measures” the A spin in the direction of the z -axis and the electromagnet \mathcal{B} “measures” the B spin in the direction of the z' -axis, which is obtained after a rotation of an angle δ around the y -axis.

In most papers on EPR-B experiment, the initial wave function of the quantum system composed of two entangled particles is the singlet spinor:

$$\Psi_0 = \frac{1}{\sqrt{2}}(|+A\rangle|-B\rangle - |-A\rangle|+B\rangle) \tag{9}$$

where $|\pm_A\rangle$ (resp. $|\pm_B\rangle$) are the eigenvectors of the spin operators S_{z_A} (resp. S_{z_B}) in the z -direction pertaining to particle A (resp.B): $S_{z_A}|\pm_A\rangle = \pm(\frac{\hbar}{2})|\pm_A\rangle$ (resp. $S_{z_B}|\pm_B\rangle = \pm(\frac{\hbar}{2})|\pm_B\rangle$).

More specifically, the initial singlet wave function has a spatial extension:

$$\Psi_0(\mathbf{r}_A, \mathbf{r}_B) = \frac{1}{\sqrt{2}}f(\mathbf{r}_A)f(\mathbf{r}_B)(|+A\rangle|-B\rangle - |-A\rangle|+B\rangle) \tag{10}$$

where $\mathbf{r} = (x, z)$ and $f(\mathbf{r}) = (2\pi\sigma_0^2)^{-\frac{1}{2}} e^{-\frac{x^2+z^2}{4\sigma_0^2}}$. This spatial extension is essential to solve correctly the Pauli equation in space. Moreover, in Bohmian mechanics, the spatial extension is necessary to take into account particle position.

In the Copenhagen interpretation, the result of the simultaneous measurement of two spins is obtained directly from the initial wave function (9) written in the basis of the eigenvectors of the measuring operators, using for this the quantum-mechanics measurement postulates. For this, we make a coordinate change of the particle B, placing it in the plane $x'Oy'$ obtained from Oz by rotation δ around Oy . So we have:

$$x_B = x'_B \cos \delta + z'_B \sin \delta \quad \text{and} \quad z_B = -x'_B \sin \delta + z'_B \cos \delta.$$

In the new basis $|\pm'_B\rangle$ of the eigenvectors of the operator $\sigma_{z'_B}$, the spinors $|\pm_B\rangle$ are written:

$$|+_B\rangle = \cos \frac{\delta}{2} |+_B'\rangle + \sin \frac{\delta}{2} |-_B'\rangle \quad \text{and} \quad |-_B\rangle = -\sin \frac{\delta}{2} |+_B'\rangle + \cos \frac{\delta}{2} |-_B'\rangle. \quad (11)$$

The initial wave function (9) is then written:

$$\Psi_0 = \frac{1}{\sqrt{2}} \left(-\sin \frac{\delta}{2} |+_A\rangle |+_B'\rangle + \cos \frac{\delta}{2} |+_A\rangle |-_B'\rangle - \cos \frac{\delta}{2} |-_A\rangle |+_B'\rangle - \sin \frac{\delta}{2} |-_A\rangle |-_B'\rangle \right). \quad (12)$$

Since, in the EPR-B experiment, A spin is measured along the z -axis and that of B along the z' -axis, the wave function (12) predicts the following probabilities for the measuring torques:

$$P(+, +) = P(-, -) = \frac{1}{2} \sin^2 \frac{\delta}{2}, \quad P(+, -) = P(-, +) = \frac{1}{2} \cos^2 \frac{\delta}{2} \quad (13)$$

where $P(+, -)$, for example, corresponds to the probability to find A with the spin up (+) and B with the spin down (-).

The same probabilities are obtained if we take the initial singlet (10) with a spatial extension. Indeed as $f(\mathbf{r}_B) = f(\mathbf{r}'_B)$, we have:

$$\Psi_0(\mathbf{r}_A, \mathbf{r}'_B) = \frac{1}{\sqrt{2}} f(\mathbf{r}_A) f(\mathbf{r}'_B) \left(-\sin \frac{\delta}{2} |+_A\rangle |+_B'\rangle + \cos \frac{\delta}{2} |+_A\rangle |-_B'\rangle - \cos \frac{\delta}{2} |-_A\rangle |+_B'\rangle - \sin \frac{\delta}{2} |-_A\rangle |-_B'\rangle \right) \quad (14)$$

and the calculation of $P(+, -)$ for example is made by integration: $P(+, -) = \int \frac{1}{2} \cos^2 \frac{\delta}{2} |f(\mathbf{r}_A)|^2 |f(\mathbf{r}'_B)|^2 d\mathbf{r}_A d\mathbf{r}'_B = \frac{1}{2} \cos^2 \frac{\delta}{2}$.

In the de Broglie–Bohm interpretation, the postulates of quantum-mechanics measurement are not used and results of the measurement are obtained by calculating

the evolution of the wave function in interaction with measuring apparatuses (see Appendix for numerical values).

Let us consider the wave function of the two particles A and B of the EPR-B experiment in the configuration space. These are two identical particles: both are electrically neutral, with magnetic moments μ , and are respectively subject to magnetic fields \mathbf{B}^A and \mathbf{B}^B . This wave function $\Psi(\mathbf{r}_A, \mathbf{r}_B, t)$ admits 4 components $\Psi^{a,b}(\mathbf{r}_A, \mathbf{r}_B, t)$ on the basis $[|\pm_A\rangle, |\pm_B\rangle]$ with $a = \pm$ and $b = \pm$, and its evolution is given by the two-body Pauli equation (see Holland [22] p. 417 and Dürr et al. [7]). In Einstein notation this is expressed as:

$$i\hbar \frac{\partial \Psi^{a,b}}{\partial t} = \left(-\frac{\hbar^2}{2m} (\nabla_A)^2 - \frac{\hbar^2}{2m} (\nabla_B)^2 \right) \Psi^{a,b} + \mu B_j^A(\mathbf{r}_A)(\sigma_j)_c^a \Psi^{c,b} + \mu B_j^B(\mathbf{r}_B)(\sigma_j)_d^b \Psi^{a,d} \tag{15}$$

with $j = 1$ to 3 . The initial conditions are:

$$\Psi^{a,b}(\mathbf{r}_A, \mathbf{r}_B, 0) = \Psi_0^{a,b}(\mathbf{r}_A, \mathbf{r}_B) \tag{16}$$

where the $\Psi_0^{a,b}(\mathbf{r}_A, \mathbf{r}_B)$ correspond to the singlet state (10).

One of the difficulties of the interpretation of the EPR-B experiment is the existence of two simultaneous measurements. By doing these measurements one after the other as proposed in 1987 by Dewdney et al. [11], it facilitates the interpretation and calculation of the experiment. That is the purpose of the two-step version of the EPR-B experiment studied below. The latter experiment is equivalent to the previous experiment and gives the usual correlations (13) of the initial EPR-B experiment.

Classic treatments of the EPR-B experiment within Bohmian mechanics [10,21,22] focus only on final calculations in order to ensure consistency with experimental results. In our view, intermediate formulas (those after the first step) are also very interesting to present. That is why we detail below the complete calculations and the conclusions after each step.

3.1 First Step: “Measurement” of A Spin

In the first step we make, on a pair of entangled particles A and B, a Stern–Gerlach “measurement” for atom A, then in the second step a Stern–Gerlach “measurement” for atom B.

Consider that at time t_0 the particle A arrives at the entrance of electromagnet \mathcal{A} . Δt is the duration of crossing electromagnet \mathcal{A} and t is the time after the \mathcal{A} exit. At time $t_0 + \Delta t + t$, wave function (10) becomes [20]:

$$\Psi(\mathbf{r}_A, \mathbf{r}_B, t_0 + \Delta t + t) = \frac{1}{\sqrt{2}} f(\mathbf{r}_B) (f^+(\mathbf{r}_A, t)|_{+A})|_{-B} - f^-(\mathbf{r}_A, t)|_{-A})|_{+B} \tag{17}$$

with

$$f^\pm(\mathbf{r}, t) \simeq f(x, z \mp z_\Delta \mp ut)e^{i(\frac{\pm mu z}{\hbar} + \varphi^\pm(t))}. \tag{18}$$

where z_Δ and u are defined in Appendix by Eq. (33).

The atomic density $\rho(z_A, z_B, t_0 + \Delta t + t)$ is found by integrating $\Psi^\dagger(\mathbf{r}_A, \mathbf{r}_B, t_0 + \Delta t + t) \times \Psi(\mathbf{r}_A, \mathbf{r}_B, t_0 + \Delta t + t)$ on x_A and x_B :

$$\begin{aligned} \rho(z_A, z_B, t_0 + \Delta t + t) &= \left((2\pi\sigma_0^2)^{-\frac{1}{2}} e^{-\frac{(z_B)^2}{2\sigma_0^2}} \right) \\ &\times \left((2\pi\sigma_0^2)^{-\frac{1}{2}} \frac{1}{2} \left(e^{-\frac{(z_A - z_\Delta - ut)^2}{2\sigma_0^2}} + e^{-\frac{(z_A + z_\Delta + ut)^2}{2\sigma_0^2}} \right) \right). \end{aligned} \tag{19}$$

Our previous studies [20] on the EPR-B experiment are based on Eqs. (17) and (19), which are not explicitly presented in the classic Bohmian framework. We deduce from (19) that the beam of particles A is divided into two parts, while the B beam of particles is not, and remains stable. Moreover, we note that the space quantization of particle A is identical to that of a free particle in a single Stern–Gerlach apparatus: the distance $\delta z = 2(z_\Delta + ut)$ between the two spots N^+ (spin +) and N^- (spin -) of a set of particles A is the same as the distance between the two spots N^+ and N^- of a set of particles in a single Stern–Gerlach experiment [18], cf. (34) in Appendix. We finally deduce from (19) that:

- the density of B is not affected by the “measurement” of A,
- the density of A is the same, whether particle A is entangled with B (19) or not.

These two results can be tested experimentally. We also conclude from (17) that the spins of A and B remain opposite throughout the experiment. This analysis of the first step was not made in the previous Bohmian approaches. It also provides the possibility of replacing the single spinor of two entangled particles with two independent single-particle spinors, plus an interaction-at-a-distance that maintains the two spin vectors in opposite directions.

3.2 Second Step: “Measurement” of B Spin.

After a first step of a Stern–Gerlach “measurement” on atom A, between t_0 and $t_1 = t_0 + \Delta t + t_D$, the second step corresponds to a Stern–Gerlach “measurement” on atom B, with an electromagnet \mathcal{B} forming an angle δ with \mathcal{A} between t_1 and $t_1 + \Delta t + t_D$.

At time t_1 , the wave function in configuration space is given by (17) with $t = t_D$. In the new basis $[|\pm_A\rangle, |\pm'_B\rangle]$, this wave function is written:

$$\begin{aligned} \Psi(\mathbf{r}_A, \mathbf{r}'_B, t_1) &= \frac{1}{\sqrt{2}} f(\mathbf{r}'_B) \left[-\sin \frac{\delta}{2} f^+(\mathbf{r}_A, t_D) |+_A\rangle |+_B'\rangle + \cos \frac{\delta}{2} f^+(\mathbf{r}_A, t_D) |+_A\rangle |-_B'\rangle \right. \\ &\quad \left. - \cos \frac{\delta}{2} f^-(\mathbf{r}_A, t_D) |-_A\rangle |+_B'\rangle - \sin \frac{\delta}{2} f^-(\mathbf{r}_A, t_D) |-_A\rangle |-_B'\rangle \right]. \end{aligned} \tag{20}$$

After the measurement of B at its exit of magnetic field \mathcal{B} , at time $t_1 + \Delta t + t_D$, the wave function (20) becomes:

$$\begin{aligned} \Psi(\mathbf{r}_A, \mathbf{r}'_B, t_1 + \Delta t + t_D) = \frac{1}{\sqrt{2}} \left[-\sin \frac{\delta}{2} f^+(\mathbf{r}_A, t_D) f^+(\mathbf{r}'_B, t_D) |+_A\rangle |+_B'\rangle \right. \\ + \cos \frac{\delta}{2} f^+(\mathbf{r}_A, t_D) f^-(\mathbf{r}'_B, t_D) |+_A\rangle |-_B'\rangle \\ - \cos \frac{\delta}{2} f^-(\mathbf{r}_A, t_D) f^+(\mathbf{r}'_B, t_D) |-_A\rangle |+_B'\rangle \\ \left. - \sin \frac{\delta}{2} f^-(\mathbf{r}_A, t_D) f^-(\mathbf{r}'_B, t_D) |-_A\rangle |-_B'\rangle \right]. \end{aligned} \quad (21)$$

Equation (21) predicts probabilities of (13). The calculation of $P(+, -)$, for example, is made by integration: $P(+, -) = \int \frac{1}{2} \cos^2 \frac{\delta}{2} |f^+(\mathbf{r}_A, t_D)|^2 |f^-(\mathbf{r}'_B, t_D)|^2 d\mathbf{r}_A d\mathbf{r}'_B = \frac{1}{2} \cos^2 \frac{\delta}{2}$.

Similarly to Holland, we obtain, for spatial quantization and correlations of spins in this two-step version of the EPR-B experiment, the same results as in the EPR-B experiment. The EPR correlations are therefore obtained only by solving the two-body Pauli equation without using the quantum-measurement postulates.

4 Two Single-Particle Spinors in the EPR-B Experiment

In this section, we present the principal contribution of the paper: how to replace the singlet spinor of EPR-B experiment with two single-particle spinors plus an interaction-at-a-distance that maintains the two spin vectors in opposite directions. When the entangled pair of particles A and B is created, we assume that each particle has the initial wave function: $\Psi_0^A(\mathbf{r}_A, \theta_0^A, \varphi_0^A)$ and $\Psi_0^B(\mathbf{r}_B, \theta_0^B, \varphi_0^B)$ like in Eq. (6):

$$\Psi_0^A(\mathbf{r}_A, \theta_0^A, \varphi_0^A) = f(\mathbf{r}_A) \left(\cos \frac{\theta_0^A}{2} |+_A\rangle + \sin \frac{\theta_0^A}{2} e^{i\varphi_0^A} |-_A\rangle \right) \quad (22)$$

and

$$\Psi_0^B(\mathbf{r}_B, \theta_0^B, \varphi_0^B) = f(\mathbf{r}_B) \left(\cos \frac{\theta_0^B}{2} |+_B\rangle + \sin \frac{\theta_0^B}{2} e^{i\varphi_0^B} |-_B\rangle \right). \quad (23)$$

Moreover those spinors have opposite spins: $\theta_0^B = \pi - \theta_0^A, \varphi_0^B = \varphi_0^A - \pi$. We treat the dependence on y classically: speed $-v_0$ for A and v_0 for B. Then the Pauli principle tells us that the two-body wave function must be antisymmetric; it is written:

$$\begin{aligned} \Psi_0(\mathbf{r}_A, \theta_A, \varphi_A, \mathbf{r}_B, \theta_B, \varphi_B) = \Psi_A^0(\mathbf{r}_A, \theta_A, \varphi_A) \Psi_B^0(\mathbf{r}_B, \theta_B, \varphi_B) \\ - \Psi_A^0(\mathbf{r}_B, \theta_B, \varphi_B) \Psi_B^0(\mathbf{r}_A, \theta_A, \varphi_A) \end{aligned}$$

i.e. $\Psi_0(\mathbf{r}_A, \theta_A, \varphi_A, \mathbf{r}_B, \theta_B, \varphi_B) = f(\mathbf{r}_A)f(\mathbf{r}_B)[(\cos \frac{\theta_A}{2}|+_A\rangle + \sin \frac{\theta_A}{2}e^{i\varphi_A}|-_A\rangle)(\cos \frac{\theta_B}{2}|+_B\rangle + \sin \frac{\theta_B}{2}e^{i\varphi_B}|-_B\rangle) - (\cos \frac{\theta_B}{2}|+_A\rangle + \sin \frac{\theta_B}{2}e^{i\varphi_B}|-_A\rangle)(\cos \frac{\theta_A}{2}|+_B\rangle + \sin \frac{\theta_A}{2}e^{i\varphi_A}|-_B\rangle)]$, and after calculation we obtain the same singlet state as (10), factor-wise:

$$\Psi_0(\mathbf{r}_A, \theta_A, \varphi_A, \mathbf{r}_B, \theta_B, \varphi_B) = -e^{i\varphi_A} f(\mathbf{r}_A)f(\mathbf{r}_B)(|+_A\rangle|-_B\rangle - |-_A\rangle|+_B\rangle)$$

The assumption of the existence of initial wave functions $\Psi_0^A(\mathbf{r}_A, \theta_0^A, \varphi_0^A)$ and $\Psi_0^B(\mathbf{r}_B, \theta_0^B, \varphi_0^B)$ (Eqs. 22, 23) is consistent with singlet state (10) and new in Bohmian interpretations. It is important to note that each entangled pair of atoms has a different value of $(\theta_0^A, \varphi_0^A)$ and thus $(\theta_0^B = \pi - \theta_0^A, \varphi_0^B = \varphi_0^A - \pi)$. At each emission of one EPR-B pair, the initial spin directions are *unknown*: θ_0^A have a uniform distribution over $[0, \pi]$ and φ_0^A have a uniform distribution over $[0, 2\pi]$, according to the invariance in all rotations in 3D space.

This interpretation differs from the classic Bohmian interpretation. Indeed, in Dewdney et al. [10,21], Bohm and Hiley [13] (p. 226) and Holland [22] (pp. 417 and 467), the spin vectors are defined by a generalization of the definition (3) applied to the singlet wave function, and no to a wave function in the 3D space. These authors find for each particle an initial spin that is strictly zero and a variation of the spin module during the experiment from 0 to $\frac{\hbar}{2}$. This solution gives mathematically a causal interpretation of the EPR-B experiment, but variability of spin module causes it to lose its physical sense.

With our assumptions, we consider two initial spin vectors \mathbf{s}^A and \mathbf{s}^B with a module $\frac{\hbar}{2}$ as in the one-body case. It is the total spin of the singlet that is equal to zero. We therefore assume that, at the initial time, we know the wave functions (22) and (23) of the particles A and B. In the de Broglie–Bohm interpretation, we assume also that the initial position of particle A is known $(x_0^A, y_0^A = 0, z_0^A)$ as well as of the particle B $(x_0^B, y_0^B = 0, z_0^B)$.

It remains to determine the evolution of these wave functions and the trajectories of particles A and B.

Let’s start with particle A. Equation (19) shows that the density of A is independent of that of B: it is equal to the density of a family of free particles in a Stern–Gerlach apparatus, whose initial spin orientation has been randomly chosen (it is exactly the density given by Eq. (34) in the Appendix). Since the particle A can be described by the initial wave function (22), we can assume that its evolution is that to a free particle in a Stern–Gerlach apparatus, i.e.:

$$\Psi^A(\mathbf{r}_A, t_0 + \Delta t + t) = \cos \frac{\theta_0^A}{2} f^+(\mathbf{r}_A, t)|+_A\rangle + \sin \frac{\theta_0^A}{2} e^{i\varphi_0^A} f^-(\mathbf{r}_A, t)|-_A\rangle \quad (24)$$

For an initial polarization $(\theta_0^A, \varphi_0^A)$ and an initial position (z_0^A) , we obtain, in the de Broglie–Bohm interpretation [13], an evolution of the position $(z_A(t))$ and of the spin orientation of A $(\theta^A(z_A(t), t))$ [18]. In the interval $[t_0, t_0 + \Delta t]$ during passage through the electromagnet, we obtain:

$$\frac{dz_A}{dt} = \frac{\mu_0 B_0 t}{m} \cos \theta(z_A, t)$$

$$\text{with } \tan \frac{\theta(z_A(t), t)}{2} = \tan \frac{\theta_0}{2} e^{-\frac{\mu_0 B_0' t^2 z_A}{2m\sigma_0^2}} \tag{25}$$

with the initial condition $z_A(t_0) = z_0^A$; and in the interval $[t_0 + \Delta t, t_0 + \Delta t + t]$ ($t \geq 0$) after passing through the electromagnet:

$$\begin{aligned} \frac{dz_A}{dt} &= u \frac{\tanh(\frac{(z_\Delta + ut)z_A}{\sigma_0^2}) + \cos \theta_0}{1 + \tanh(\frac{(z_\Delta + ut)z_A}{\sigma_0^2}) \cos \theta_0} \\ \text{and } \tan \frac{\theta(z_A(t), t)}{2} &= \tan \frac{\theta_0}{2} e^{-\frac{(z_\Delta + ut)z_A}{\sigma_0^2}}. \end{aligned} \tag{26}$$

It is this evolution of the polarization which is shown in Fig. 1 for the initial polarization ($\theta_0 = \frac{\pi}{3}$). The behavior of particle A is independent of B, whether the particle is entangled or not.

Let us now study particle B. Equation (19) shows that the density of B is independent of time and of the density of A: it is equal to the density of a family of free particles, which is constant in x and z . Therefore we can assume that the particle B is immobile in x and z : $z_B(t) = z_0^B$ and $x_B(t) = x_0^B$. Moreover, B follows a rectilinear classical trajectory in y with $y_B(t) = v_0 t$.

Equation (17) shows that spins of A and B remain opposite throughout step 1. The spin of a particle A is oriented gradually following the position of the particle. The spin of particle B follows that of A, while remaining opposite. Therefore, we can assume that the orientation of B spin is driven by the orientation of A spin, like an interaction-at-a-distance:

$$\theta^B(t) = \pi - \theta(z_A(t), t) \quad \text{and} \quad \varphi^B(t) = \varphi(z_A(t), t) - \pi. \tag{27}$$

Since the particle B can be described by the initial wave function (23), we can then associate to the particle B the wave function:

$$\Psi^B(\mathbf{r}_B, t_0 + \Delta t + t) = f(\mathbf{r}_B) \left(\cos \frac{\theta^B(t)}{2} |+_B\rangle + \sin \frac{\theta^B(t)}{2} e^{i\varphi^B(t)} |-_B\rangle \right). \tag{28}$$

This wave function is specific, because it depends upon initial conditions of A (positions and spins). The orientation of B spin is driven by that of particle A *through the singlet wave function*. Thus, the singlet wave function is the non-local hidden variable.

Finally, during the first step, the singlet spinor in configuration space (17) can be replaced by the two single-particle spinors given by Eqs. (24) and (28).

After the “measurement” of A at time $t_1 = t_0 + \Delta t + t_D$, if the A measurement is + (respectively -), i.e. $\theta(z_A(t), t) = +\frac{\pi}{2}$ (resp. $-\frac{\pi}{2}$), we can deduce from Eqs. (27) and (28) that:

$$\Psi^B(\mathbf{r}_B, t_1) = f(\mathbf{r}_B) e^{i\varphi^B(t_1)} |-_B\rangle \quad (\text{resp. } f(\mathbf{r}_B) |+_B\rangle) \tag{29}$$

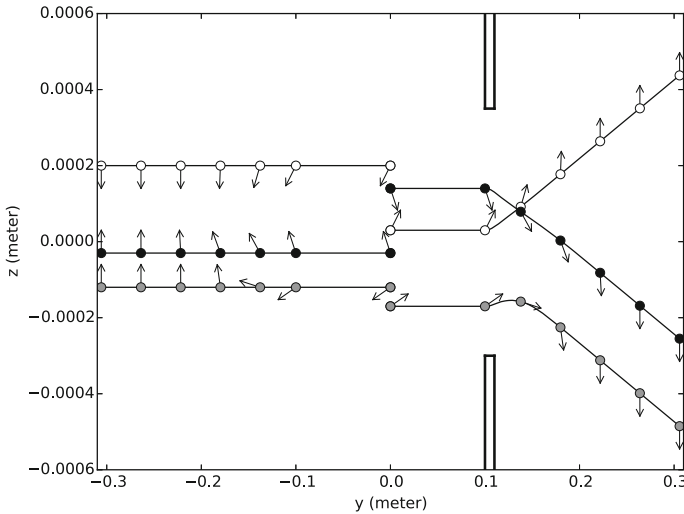


Fig. 3 Evolution of the trajectories and the spin orientations (*arrow*) of three pairs of entangled A-B atoms (represented in *black, gray and white*) in the first step of the EPR-B experiment. There are created at the initial moment in $y = 0$ ($y_0^A = y_0^B = 0$). z_0^A and z_0^B have been randomly chosen. θ_0^A is also randomly chosen, θ_0^B is in opposition to θ_0^A , i.e.: $\theta_0^B = \pi - \theta_0^A$. Particle A goes to the right and cross a Stern-Gerlach device. Particle B goes to the left without crossing any device. The spin orientation along a trajectory (θ) is indicated by an *arrow*

We have also $x^B(t_1) = x_0^B$ and $x^B(t_1) = z_0^B$. After this first “measurement”, the second step of the EPR-B experiment is exactly the case of a single particle in a Stern-Gerlach magnet \mathcal{B} which is at an angle δ (resp. $\pi - \delta$) in relation to \mathcal{A} .

Figure 3 represents the evolution of trajectories and the spin orientations of three pairs of entangled A–B atoms in the first step of the EPR-B experiment. The three pairs of A–B particles are represented in black, gray and white on the figure. There are created at the initial moment in $y = 0$ ($y_0^A = y_0^B = 0$). The respective positions of A and B in relation to z , z_0^A and z_0^B , at the initial moment have been randomly chosen. The orientation of the spin of A at the initial moment, θ_0^A , is randomly chosen, in opposition to B, i.e.: $\theta_0^B = \pi - \theta_0^A$ (and $\varphi_0^B = \varphi_0^A - \pi$). Particle A goes to the right and cross a Stern–Gerlach device. Particle B goes to the left without crossing any device. The spin orientation (θ) is indicated by an *arrow*: the arrows on the right (respectively on the left) represent the evolution of the spin orientation of A (respectively of B).

5 Conclusion

We first recalled the definition of the spin vector in Bohmian mechanics (dependent on both wave function and position) and its evolution during the phenomenon of measurement. In Bohmian mechanics, the “measured” value is not a preexisting value. It is the value obtained after a continuous orientation of the spin, either in the direction of the magnetic field gradient, or in the opposite direction.

Next, we have shown that, for the two entangled particles of the two-step version of the EPR-B experiment, it is possible to replace the singlet spinor in configuration space (17) by two single-particle spinors in physical space, given by Eqs. (24) and (28).

We have demonstrated that the “first-measured” particle A behaves in a Stern–Gerlach apparatus as if it were not entangled. During the measurement of A, the particle density of B evolves as if it were not entangled. These two properties could be tested experimentally when the EPR-B experiment can be carried out easily. This result was obtained in the de Broglie–Bohm interpretation using an integration of the two-body Pauli equation over time and space from an initial singlet with a spatial extension (10).

As de Broglie and Schrödinger stated at the Solvay Conference in 1927, the wave function in configuration space may only be a mathematical tool that can be replaced by more physical wave functions. In our model, the A wave function is the same as that of a free particle in a Stern–Gerlach apparatus, the B wave function is the same as that of a free particle whose spin orientation vector is driven by the orientation of the A spin. Thus, we obtain a possible physical understanding of the EPR-B experience and the entanglement.

Our interpretation goes beyond the limit of the one put forward by Dewdney, Holland and Kyprianidis [10], where EPR-B spins evolved from 0 to $\frac{\hbar}{2}$ from creation to measurement, which fits badly with spin quantification. We thus make the de Broglie–Bohm interpretation more credible.

These results also reopen the discussion about the completeness of quantum mechanics and the existence of hidden variables. Firstly, it clearly shows that Bohmian mechanics, which only uses resolution of the Pauli equation, gives the same statistical results as the Copenhagen interpretation for the Stern–Gerlach and EPR-B experiments. It is the two-body Pauli equation that couples spin and spatial degrees of freedom in Eqs. (17) and (21). Moreover, the measurement postulates and the postulate of wave packet reduction are not used in Bohmian mechanics and we show that they can be demonstrated (cf. Appendix).

The wave function of the singlet state alone introduces non locality: when we replace a singlet wave function in the configuration space with two wave functions in the 3D physical space, we must introduce *interaction-at-a-distance* (Eq. 27) between the A spin orientation and that of B.

Thus, the non-local influence in the EPR-B experiment only concerns the spin orientation, not the motion of the particles themselves. This is a key point in the search for a physical understanding of this non-local influence.

Acknowledgments Authors gratefully acknowledge the two anonymous reviewers for their useful comments and constructive suggestions which helped to improve the paper.

Appendix: Spin “Measurement ” in the Stern–Gerlach Experiment

The measurement of spin of a silver atom is carried out by a Stern–Gerlach apparatus: an electromagnet *A*, where there is a strongly inhomogeneous magnetic field, followed by a screen *P* (Fig. 4). In the Stern–Gerlach experiment, silver atoms contained in

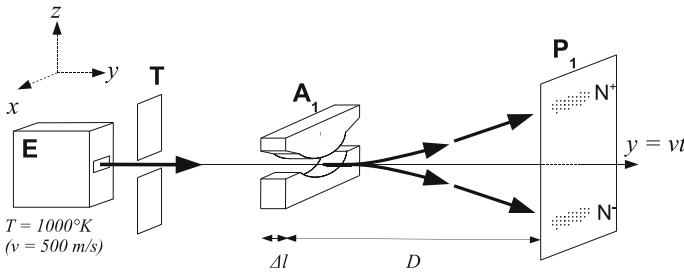


Fig. 4 Schematic configuration of a Stern–Gerlach apparatus

the oven E are heated to a high temperature and escape through a narrow opening. A second aperture, T, selects those atoms whose velocity, v_0 , is parallel to the y-axis. The atomic beam passes through the gap of the electromagnet A, before condensing on the screen P on two spots of equal intensity N^+ and N^- . The magnetic moment of each silver atom before crossing the electromagnet is oriented randomly (isotropically).

In the beam, we represent the atoms by their wave function; one can assume that at the entrance to the electromagnet A (at the initial time $t = 0$), each atom can be approximatively described by a Gaussian spinor in x and z :

$$\Psi^0(x, z) = (2\pi\sigma_0^2)^{-\frac{1}{2}} e^{-\frac{x^2+z^2}{4\sigma_0^2}} \begin{pmatrix} \cos \frac{\theta_0}{2} e^{i\frac{\varphi_0}{2}} \\ \sin \frac{\theta_0}{2} e^{-i\frac{\varphi_0}{2}} \end{pmatrix} \tag{30}$$

corresponding to a pure state. The variable y is treated in a classical way with $y = v_0t$.

In (30), θ_0 and φ_0 characterize the initial orientation of the spin. This initial orientation being randomized, one may suppose that θ_0 is drawn in a uniform law from $[0, \pi]$ and that φ_0 is drawn in a uniform law from $[0, 2\pi]$; In this way, we obtain a beam of atoms in which each atom has a different spinor: this is a model of a mixture of pure states.

In the Copenhagen interpretation, it is not necessary to resolve the Pauli equation. Just applying the postulates of quantum-mechanics measurement is sufficient. For measurement of the spin along the z -axis, the postulate of quantification states that the measurement corresponds to an eigenvalue of the spin operator $S_z = \frac{\hbar}{2}\sigma_z$, and the spectral decomposition postulate states that Eq. (7) gives probability $\cos^2\frac{\theta}{2}$ (resp. $\sin^2\frac{\theta}{2}$) to measure the particle in the spin state $+\frac{\hbar}{2}$ (resp. $-\frac{\hbar}{2}$).

In the de Broglie–Bohm interpretation, the postulates of quantum mechanics measurement are not used, but demonstrated (see below). The results of the measurement are obtained, first by calculating the evolution of the wave function in interaction with the measuring apparatus with the Pauli equation (Eq. 1), secondly by using the calculation of the wave function in space and time to pilot the particle (Eq. 2).

Let us consider the evolution of the initial wave function (5) in the Stern–Gerlach apparatus. To obtain an explicit solution to the Stern–Gerlach experiment, we take the numerical values used in the Cohen–Tannoudji textbook [15]. For a silver atom, we have $m = 1.8 \times 10^{-25}$ kg, $v_0 = 500$ m/s, $\sigma_0 = 10^{-4}$ m. For the electromagnetic field \mathbf{B} , $B_x = B'_0x$; $B_y = 0$ and $B_z = B_0 - B'_0z$ with $B_0 = 5$ T, $B'_0 = \left| \frac{\partial B}{\partial z} \right| = - \left| \frac{\partial B}{\partial x} \right| = 10^3$ T/m over a length $\Delta l = 1$ cm.

The variable y will be treated classically with $y = v_0 t$. The particle stays within the magnetic field for a time $\Delta t = \frac{\Delta l}{v_0} = 2 \times 10^{-5} s$. On exiting the magnetic field, the particle is free until it reaches screen P placed at a $D = 20$ cm distance.

During this time $[0, \Delta t]$, the spinor is calculated (Dürre et al. [7], Gondran [18]) with the Pauli equation (1), where $\mu = \frac{e\hbar}{2m_e}$ is the Bohr magneton:

$$\Psi(x, z, t) \simeq \begin{pmatrix} \cos \frac{\theta_0}{2} (2\pi\sigma_0^2)^{-\frac{1}{2}} e^{-\frac{(z - \frac{\mu_B B'_0}{2m} t^2)^2 + x^2}{4\sigma_0^2}} e^{i \frac{\mu_B B'_0 t z - \frac{\mu_0^2 B_0'^2}{6m} t^3 + \mu_B B_0 t + \frac{\hbar\varphi_0}{2}}}{i \sin \frac{\theta_0}{2} (2\pi\sigma_0^2)^{-\frac{1}{2}} e^{-\frac{(\frac{\mu_B B'_0}{2m} t^2)^2 + x^2}{4\sigma_0^2}} e^{i \frac{-\mu_B B'_0 t z - \frac{\mu_0^2 B_0'^2}{6m} t^3 - \mu_B B_0 t - \frac{\hbar\varphi_0}{2}}}{\end{pmatrix} \tag{31}$$

After the magnetic field, at time $t + \Delta t$ ($t \geq 0$), in the free space, the spinor becomes [18]

$$\Psi(x, z, t + \Delta t) \simeq \begin{pmatrix} \cos \frac{\theta_0}{2} (2\pi\sigma_0^2)^{-\frac{1}{2}} e^{-\frac{(z - z_\Delta - ut)^2 + x^2}{2\sigma_0^2}} e^{i \frac{muz + \hbar\varphi_+}{\hbar}}}{i \sin \frac{\theta_0}{2} (2\pi\sigma_0^2)^{-\frac{1}{2}} e^{-\frac{(z + z_\Delta + ut)^2 + x^2}{2\sigma_0^2}} e^{i \frac{-muz + \hbar\varphi_-}{\hbar}}}{\end{pmatrix} \tag{32}$$

where

$$z_\Delta = \frac{\mu_B B'_0 (\Delta t)^2}{2m} = 10^{-5} m, \quad u = \frac{\mu_B B'_0 (\Delta t)}{m} = 1 m/s. \tag{33}$$

Equation (32) takes into account the spatial extension of the spinor and we note that the two-spinor components have very different values.

Since we have a mixture of pure states, the atomic density $\rho(z, t + \Delta t)$ is found by integrating $\rho(x, z, t + \Delta t)$ on x and on (θ_0, φ_0) :

$$\rho(z, t + \Delta t) = (2\pi\sigma_0^2)^{-\frac{1}{2}} \frac{1}{2} \left(e^{-\frac{(z - z_\Delta - ut)^2}{2\sigma_0^2}} + e^{-\frac{(z + z_\Delta + ut)^2}{2\sigma_0^2}} \right). \tag{34}$$

The decoherence time t_D , where the beam is separated into the two spots N^+ and N^- (when $z_\Delta + ut_D \geq 3\sigma_0$), is then given by the equation:

$$t_D \simeq \frac{3\sigma_0 - z_\Delta}{u} = 3 \times 10^{-4} s. \tag{35}$$

We then obtain atoms with spins oriented only along the z -axis (positively or negatively). Experimentally, we do not measure the spin directly, but position (\tilde{x}, \tilde{z}) of the particle impact on P . If $\tilde{z} \in N^+$, the term ψ^- of (32) is numerically equal to zero, and the spinor Ψ is proportional to $\begin{pmatrix} 1 \\ 0 \end{pmatrix}$, one of the eigenvectors of σ_z :

$$\Psi(\tilde{z}, t + \Delta t) \simeq (2\pi\sigma_0^2)^{-\frac{1}{4}} \cos \frac{\theta_0}{2} e^{-\frac{(\tilde{z} - z_\Delta - ut)^2 + \tilde{x}^2}{4\sigma_0^2}} e^{i \frac{mu\tilde{z} + \hbar\varphi_+}{\hbar}} \begin{pmatrix} 1 \\ 0 \end{pmatrix}.$$

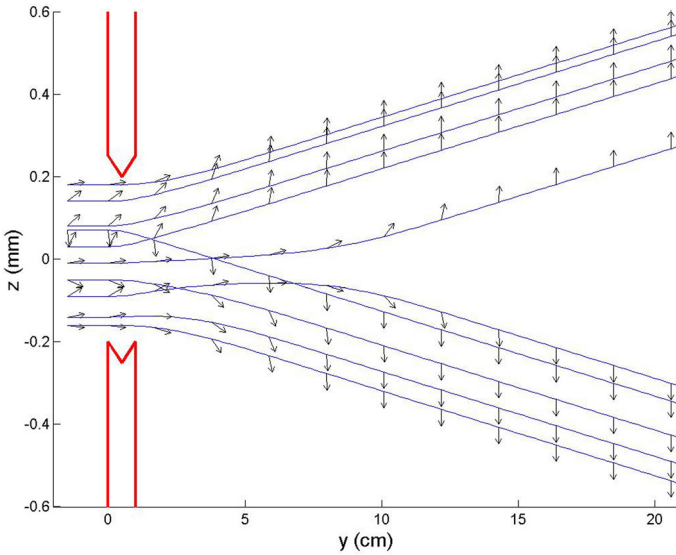


Fig. 5 10 silver atom trajectories after the electro-magnet where the initial characteristics $(\theta_0, \varphi_0, z_0)$ have been randomly chosen; *Arrows* represent the spin orientation $\theta(z(t), t)$

If $\tilde{z} \in N^-$, the term ψ^+ of (32) is numerically equal to zero and the spinor Ψ is proportional to $\begin{pmatrix} 0 \\ 1 \end{pmatrix}$, the other eigenvector of σ_z :

$$\Psi(\tilde{z}, t + \Delta t) \simeq (2\pi\sigma_0^2)^{-\frac{1}{4}} \sin \frac{\theta_0}{2} e^{-\frac{(\tilde{z}+z_\Delta+ut)^2+\tilde{x}^2}{4\sigma_0^2}} e^{i\frac{-mu\tilde{z}+h\varphi_-}{\hbar}} \begin{pmatrix} 0 \\ 1 \end{pmatrix}.$$

Therefore, the measurement of the spin corresponds to an eigenvalue of the spin operator $S_z = \frac{\hbar}{2}\sigma_z$. It is a proof of the postulate of quantization in Bohmian mechanics.

Equation (32) gives the probability $\cos^2 \frac{\theta_0}{2}$ (resp. $\sin^2 \frac{\theta_0}{2}$) of measuring the particle in the spin state $+\frac{\hbar}{2}$ (resp. $-\frac{\hbar}{2}$). It is a proof of the spatial decomposition postulate in Bohmian mechanics.

Figure 5 presents in x_0y a set of 10 silver-atom trajectories of which initial characteristics $(\theta_0, \varphi_0, z_0)$ have been randomly chosen: θ_0 and φ_0 , which define on one hand the wave function, have uniform distributions, and z_0^A , which on the other hand defines the particle position in the wave function, has a normal distribution $\mathcal{N}(0, \sigma_0)$. This double representation of quantum particles allows to take into account a mixture of pure states which satisfies the density of (34). Spin orientation $\theta(z(t), t)$ is represented by arrows.

We can see that the final orientation, obtained after the decoherence time t_D , will depend on the initial particle position z_0^A in the wave packet and on the initial angle θ_0^A of the atom magnetic moment with the z axis.

Finally, we can also give a clear explanation of the Albert’s example on contextuality [23, pp. 153–155]. He considers a Stern–Gerlach experiment where the initial wave function is a pure state with symmetric spin orientation ($\theta_0 = \frac{\pi}{4}$ and so $z^{\theta_0} = 0$). He

changes, in a second experiment, the orientation of the magnetic field inside the Stern–Gerlach apparatus (\mathbf{B} into $-\mathbf{B}$). For the same initial position of atoms (for example $z_0 > 0$), the first experiment gives a spin $+$ and, in the second, a spin $-$. Bohmian mechanics explains this result: u and z_Δ are proportional to $B'_0 = \frac{\partial B_z}{\partial z}$ (Eq. 33), and therefore change their signs like \mathbf{B} . By solving the Pauli equation, Bohmian mechanics is naturally contextual (involves the measuring device).

References

- Norsen, T.: The theory of (exclusively) local beables. *Found. Phys.* **40**, 1858–1884 (2010)
- Noren, T., Marian, D., Oriols, X.: Can the wave function in configuration space be replaced by single-particle wave function in physical space? *Synthese* **192**, 3125–3151 (2015)
- de Broglie, L.: *La Nouvelle Dynamique des quanta*. In: *Electrons et Photons, Rapports du Cinquième Conseil de Physique Solvay*, pp. 118–119. Gauthier-Villard, Paris (1928). Translated in [5], *The New Dynamics of Quanta*, 385
- Schrödinger, E.: *La mécanique des ondes*. In: *Electrons et Photons, Rapports du Cinquième Conseil de Physique Solvay*, pp. 118–119. Gauthier-Villard, Paris (1928). Translated in [5], *The Mechanics of Waves*, 447
- Bacciagaluppi, G., Valentini, A.: *Quantum Theory at the Crossroads*. Cambridge University Press, Cambridge (2009). [arXiv:quant-ph/0609184](https://arxiv.org/abs/quant-ph/0609184)
- Dürr, D., Goldstein, S., Zanghi, N.: Quantum equilibrium and the origin of absolute uncertainty. *J. Stat. Phys.* **67**, 843–907 (1992)
- Dürr, D., Goldstein, S., Zanghi, N.: Quantum equilibrium and the role of operators as observables in quantum theory. *J. Stat. Phys.* **116**, 959–1055 (2004)
- Takabayasi, T.: The vector representation of spinning particle in quantum theory. *Prog. Theor. Phys.* **14**, 283–302 (1955)
- Bohm, D., Schiller, R., Tiommo, J.: A causal interpretation of the Pauli equation. *Supplemento al Nuovo Cimento* **1**, 48–66 (1955)
- Dewdney, C., Holland, P.R., Kyprianidis, A.: A causal account of non-local Einstein–Podolsky–Rosen spin correlations. *J. Phys. A Math. Gen.* **20**, 4717–4732 (1987)
- Dewdney, C., Holland, P.R., Kyprianidis, A.: What happens in a spin measurement? *Phys. Lett.* **11A9**, 259–267 (1986)
- Kochen, S., Specker, E.: The problem of hidden variables in quantum mechanics. *J. Math. Mech.* **17**, 59–87 (1967)
- Bohm, D., Hiley, B.J.: *The Undivided Universe*. Routledge, London (1993)
- Feynman, R.P., Leighton, R.B., Sands, M.: *The Feynman Lectures on Physics*. Addison-Wesley, New York (1965)
- Cohen-Tannoudji, C., Diu, B., Laloë, F.: *Quantum Mechanics*. Wiley, New York (1977)
- Sakurai, J.J.: *Modern Quantum Mechanics*. Addison-Wesley, Reading (1985)
- Le Ballac, M.: *Quantum Physics*. Cambridge University Press, Cambridge (2006)
- Gondran, M., Gondran, A.: A complete analysis of the Stern–Gerlach experiment using Pauli spinors. (2005). [arXiv:quant-ph/0511276](https://arxiv.org/abs/quant-ph/0511276)
- Gondran, M., Gondran, A., Kenoufi, A.: Decoherence time and spin measurement in the Stern–Gerlach experiment. *AIP Conf. Proc.* **1424**, 116–120 (2012)
- Gondran, M., Gondran, A.: A new causal interpretation of the EPR-B experiment. *AIP Conf. Proc.* **1508**, 370 (2012)
- Dewdney, C., Holland, P.R., Kyprianidis, A., Vigier, J.P.: Spin and non-locality in quantum mechanics. *Nature* **336**, 536–544 (1988)
- Holland, P.R.: *The Quantum Theory of Motion*. Cambridge University Press, Cambridge (1993)
- Albert, D.: *Quantum Mechanics and Experience*. Harvard University Press, Cambridge (1992)